HHS Public Access

Author manuscript

Dev Cell. Author manuscript; available in PMC 2024 March 13.

Published in final edited form as:

Dev Cell. 2023 March 13; 58(5): 348–360.e6. doi:10.1016/j.devcel.2023.02.003.

Endothelial cells and Leptin Receptor+ cells promote the maintenance of stem cells and hematopoiesis in early postnatal murine bone marrow

Nergis Kara[1,#], **Yuanyuan Xue**[1,#], **Zhiyu Zhao**[1], **Malea M. Murphy**[2], **Stefano Comazzetto**[1], **Ashley Lesser**[1], **Liming Du**[1], **Sean J. Morrison**[1,3,*]

[1]Children's Research Institute and the Department of Pediatrics, University of Texas Southwestern Medical Center, Dallas, TX 75390, USA

[2]Department of Medical Physiology, Texas A&M School of Medicine, Bryan, Texas, 77807

[3]Howard Hughes Medical Institute, University of Texas Southwestern Medical Center, Dallas, TX 75390, USA

Abstract

Mammalian hematopoietic stem cells (HSCs) colonize the bone marrow during late fetal development and this becomes the major site of hematopoiesis after birth. However, little is known about the early postnatal bone marrow niche. We performed single cell RNA-sequencing of mouse bone marrow stromal cells at 4 days, 14 days, and 8 weeks after birth. Leptin Receptor-expressing ($LepR^+$) stromal cells and endothelial cells increased in frequency during this period and changed their properties. At all postnatal stages, $LepR^+$ cells and endothelial cells expressed the highest *Stem Cell Factor* (*Scf*) levels in the bone marrow. $LepR^+$ cells expressed the highest *Cxcl12* levels. In early postnatal bone marrow, SCF from $LepR^+/Prx1^+$ stromal cells promoted myeloid and erythroid progenitor maintenance while SCF from endothelial cells promoted HSC maintenance. Membrane bound SCF in endothelial cells contributed to HSCs maintenance. $LepR^+$ cells and endothelial cells are thus important niche components in early postnatal bone marrow.

eTOC

LepR+ stromal cells and endothelial cells express the highest *Scf* levels in early postnatal bone marrow. Kara and Xue et al. show these cells are necessary sources of SCF for progenitors and HSCs in early postnatal bone marrow and that they change their properties in the weeks after birth.

*Lead contact: Sean.Morrison@UTSouthwestern.edu.

#These authors contributed equally

AUTHOR CONTRIBUTIONS

N.K., and S.J.M. conceived the project, designed and interpreted experiments. N.K. and Y.X. performed most of the experiments, with technical assistance from S.C., A.L. and L.D.. Z.Z. performed bioinformatic analyses for the scRNA-seq data and statistical analyses. M.M. performed confocal imaging of half bones and analyzed the localization of HSCs.

DECLARATION OF INTERESTS

The authors declare no competing interests.

Keywords

Stromal cells; Stem Cell Factor; niche; erythropoiesis; myelopoiesis

INTRODUCTION

Hematopoietic stem cells (HSCs) arise from hemogenic endothelium in mammalian embryos [1–3], then engage in hematopoiesis in the fetal liver during mid-gestation before colonizing the bone marrow during late fetal development [4]. Postnatally, the bone marrow becomes the primary site of HSC maintenance and hematopoiesis. In adult bone marrow, HSCs are maintained within perisinusoidal niches [5–11] in which Leptin Receptor expressing ($LepR^+$) mesenchymal stromal cells and endothelial cells are necessary sources of factors for HSC maintenance, including Stem Cell Factor (SCF) [12–14], Cxcl12 [15,16], and pleiotrophin [17]. $LepR^+$ cells and endothelial cells also regulate vascular regeneration by synthesizing Angiopoietin-1 [18] and VEGF-C [19]. Recent single-cell RNA sequencing (scRNA-seq) studies of bone marrow stromal cells also found that $LepR^+$ cells and endothelial cells express the highest levels of *Scf* and *Cxcl12* in adult bone marrow [20–24].

Much less is known about the stroma and the HSC niche in early postnatal bone marrow. There is evidence that it may differ from adult bone marrow. $LepR^+$ bone marrow cells arise perinatally from chondrocytes and perichondrium in developing bones and are initially rare, found only in the metaphysis, before expanding throughout the bone marrow by adulthood [25–29]. Nestin is broadly expressed by endothelial cells in early postnatal bone marrow [26,30] but becomes more restricted to a subset of periarteriolar endothelial cells and stromal cells in adult bone marrow [31,32]. Deletion of *Cxcl12* with *Nestin-CreER* at postnatal day 7 depletes HSCs, suggesting that these cells contribute to the niche in early postnatal bone marrow [33]; however, deletion of *Cxcl12* or *Scf* with *Nestin-cre* or *Nestin-CreER* has no effect on HSC frequency or hematopoiesis in adult bone marrow [12,15]. Similarly, deletion of *Cxcl12* with *Neuron-glial antigen 2* (*NG2*)-*CreER* beginning at postnatal day 14 (P14) depletes HSCs in adult bone marrow [31] while deletion beginning at 6 weeks of age has no effect [8]. These studies raise the possibility that $NG2^+$ cells may be more important in early postnatal as compared to adult bone marrow.

RESULTS

The stromal cell composition of bone marrow changes in the weeks after birth

We performed single cell RNA sequencing (scRNA-seq) on $CD45^-Lineage^-CD71^-$ bone marrow stromal cells from P4, P14, and 8 week-old mice (Figure 1A). These cells represented 2.8%, 0.89%, and 0.59% of enzymatically dissociated bone and bone marrow cells from P4, P14, and 8 week-old mice, respectively (Figure S1A–C). At each stage, entire femurs and tibias were crushed and enzymatically dissociated. After quality filtering of the sequence data, we included in the analysis a total of 11,428 cells from 3 mice at P4, 8,020 cells from 3 mice at P14, and 4,209 cells from 4 adult mice. We detected transcripts encoded by a median of 2468, 3063, and 1845 genes per cell at P4, P14 and 8 weeks, respectively.

Unsupervised clustering of all of the data identified 16 clusters of stromal cells (Figure S1D). We visualized the clusters using Uniform Manifold Approximation and Projection (UMAP) (Figure 1B–D). Cell identity was assigned to each cluster based on differential expression of known marker genes (Figures 1C and S1E–N). The 16 cell populations and key markers used to infer cell identity are listed in Table S1. We performed SingleCellNet[34] to compare our cell clustering with that of Baryawno et al., 2019[21]. Most cell clusters we identified were highly overlapping and similarly named as the clusters identified by Baryawno et al (Figure S2A).

We observed dramatic changes in the frequencies of stromal cell populations over time as a percentage of all stromal cells (Table S1). LepR$^+$ cells (cluster 11, ref[12]), LepR$^+$Osteolectin$^+$ cells (LepR$^+$Oln$^+$; cluster 12, ref[35]), arteriolar endothelial cells (cluster 13), and sinusoidal endothelial cells (cluster 14) all increased in frequency from P4 to adult bone marrow (Table S1). The frequency of all LepR$^+$ cells increased from 0.7% of stromal cells in P4 bone marrow to 11% of stromal cells in adult bone marrow (Figure 1E). Conversely, fibroblast clusters 1–3 (clusters 8 to 10) declined in frequency (Table S1). Some osteolineage and chondrocyte lineage clusters increased and some decreased in frequency (Table S1).

LepR$^+$ cells were mainly contained within clusters 11 and 12 at each stage, though rare cells that expressed low levels of *Lepr* were also scattered among other cell populations, mainly in sinusoidal endothelial and chondrocyte cell clusters (Figures 1E and S2B). To test whether these low levels of *Lepr* expression translated into detectable LepR expression, we performed immunofluorescence analysis using anti-LepR antibody in chondrocytes and endothelial cells (Figure S2C and S2D). We did not detect any LepR staining in chondrocytes (Figure S2C). LepR staining was detected in a small minority (2.7 to 5.8%) of endothelial cells (Figure S2D–F). Since Lepr-cre does not detectably recombine in endothelial cells[12], the few endothelial cells that stained with anti-LepR antibody may have expressed truncated isoforms of *Lepr*[36,37] that would not lead to Cre expression (the Lepr-cre allele was made by inserting Cre into the 3' end of the gene such that Cre transcription requires expression of the full length isoform of *Lepr*[38]).

Nestin$^+$ cells were scattered within multiple cell clusters, including in osteolineage cells, fibroblasts, arteriolar endothelial cells, sinusoidal endothelial cells, *Smooth Muscle Actin*+ (*SMA*)$^+$ pericytes, and Schwann cells (Figure 1F and Figure S3A). *Nestin*$^+$ cells accounted for 6.2% of stromal cells in P4 bone marrow and 11% of stromal cells in adult bone marrow. *NG2*$^+$ cells were broadly distributed across osteolineage, chondrocyte, fibroblast, and *SMA*$^+$ pericyte cell clusters (Figure 1G and Figure S3B). *NG2*$^+$ cells represented 53% of stromal cells in P4 bones/bone marrow and 39% of stromal cells in adult bones/bone marrow.

Scf and *Cxcl12* are most highly expressed by LepR$^+$ cells and endothelial cells

Scf was most highly expressed by *Lepr*$^+$ cells (clusters 11 and 12) at all stages, with lower levels of expression in arteriolar endothelial cells (cluster 13), sinusoidal endothelial cells at P4 (cluster 14), and *SMA*$^+$ pericytes (cluster 15) (Figure 2B and 2D; see all clusters in Figure S3C). We observed little *Scf* expression in *Nestin*$^+$ cells or *NG2*$^+$ cells, and virtually none in osteoblasts (Figure 2D). *Cxcl12* was also most highly expressed by *Lepr*$^+$ cells at all stages, with lower levels of expression in *SMA*$^+$ cells, *Nestin*$^+$ cells, *NG2*$^+$ cells, and

endothelial cells (Figure 2C and 2E). *Cxcl12* was expressed at low levels in some fibroblast, Schwann cell, and chondrocyte cell clusters (Figure S3D). *Scf* and *Cxcl12* were thus most highly expressed by LepR$^+$ cells, endothelial cells, and SMA$^+$ cells in P4 and P14 bone marrow.

Lepr$^+$ cells undergo changes during the transition to adulthood

LepR$^+$ bone marrow stromal cells arise from chondrocytes and perichondrial cells during the first few months after birth[28,29]. We performed pseudotime trajectory analysis (Monocle 3) on all osteochondrondral cell clusters in the scRNA-seq analysis, including chondrocytes, osteoblasts, osteolineage cells, LepR$^+$ cells, and LepR$^+$Oln$^+$ cells (Figure S3E–H). The analysis showed chondrocytes at one end of the pseudotime trajectory and LepR$^+$ cells at the other end at P14 and 8 weeks of age. This analysis suggested that osteolineage and LepR$^+$Oln$^+$ cell clusters were intermediates in the differentiation of chondrocytes into LepR$^+$ cells. It was not clear what cluster contained perichondral cells. At P4, the pseudotime trajectory analysis did not identify a clear lineage relationship between chondrocytes and LepR$^+$ cells, perhaps because few LepR$^+$ cells have arisen from chondrocytes at this stage and the intermediate cell populations were rare.

Lepr$^+$ cells increased in number in the bone marrow between P4 and 8 weeks of age (Figure 1E). To test whether these cells changed their properties during this period, we performed gene ontology (GO) term enrichment analysis on genes that were differentially expressed between *Lepr*$^+$ (cluster 11) cells from P4 versus 8 week-old bone marrow. GO terms related to ribosome biogenesis and translation were enriched in P4 LepR$^+$ cells (Figure S3I) while GO terms related to the regulation of hematopoiesis, antigen processing, and inflammatory responses were enriched among 8 week-old LepR$^+$ cells (Figure S3J). The enrichment of terms related to ribosome biogenesis and protein synthesis in P4 LepR$^+$ cells suggested that these cells might be more anabolic and more mitotic than 8 week-old LepR$^+$ cells. To test this, we analyzed the incorporation of a 2 hour pulse of BrdU into LepR$^+$ bone marrow cells in P6, P14, and 8 week-old mice. P6 LepR$^+$ cells were significantly more likely to incorporate a 2 hour pulse of BrdU (5.7±1.4%) than 8 week-old LepR$^+$ cells (0.72±0.41%) (Fig. 2F–H). Therefore, one of the differences between neonatal LepR$^+$ cells and 8 week old LepR$^+$ cells is that the neonatal LepR$^+$ cells are more rapidly dividing. This likely contributes to the increase in the number of these cells in the weeks after birth (Figure 1E).

GO terms related to hematopoiesis, antigen processing, and inflammatory responses were enriched in 8 week-old LepR$^+$ cells. Many secreted factors that regulate hematopoiesis and inflammation, as well as antigen presentation genes, were more highly expressed in 8 week-old LepR$^+$ cells as compared to P4 LepR$^+$ cells (Figure S3K). The secreted factors that were more highly expressed in 8 week-old LepR$^+$ cells included factors that are known to regulate hematopoiesis, such as Csf1[39] and IL-7[40] as well as factors that regulate bone marrow inflammation, such as Adiponectin[41] and Cxcl10[42–44]. Gene products that regulate antigen presentation that were more highly expressed by 8 week-old LepR$^+$ cells included beta-2-microglobulin and 6 major histocompatibility alleles (Figure S3K). These data suggest that the transition into adulthood is marked by immunological maturation of LepR$^+$ cells and

increased ability to regulate hematopoiesis and the inflammatory environment in the bone marrow.

Nestin$^+$ cells are not a major source of SCF in early postnatal bone marrow

The scRNA-seq analysis suggested that *Nestin*$^+$ cells were not one of the main sources of *Scf* or *Cxcl12* in early postnatal or adult bone marrow (Figure 2D and 2E). Comparison of *Nestin* expression with *Scf* and *Cxcl12* expression across cell clusters showed limited overlap, and only in the *SMA*$^+$ pericyte and endothelial cell clusters, which expressed lower levels of both factors than the *Lepr*$^+$ cell clusters (Figure S3A, S3C, and S3D). Indeed, *Nestin* was detected in only a minority of cells in the *SMA*$^+$ pericyte and endothelial cell clusters (Figure 1F) so it did not mark all of the *Scf*-expressing cells within these clusters.

To independently investigate this, we generated *Nestin-CreER*; *tdTomato*; *Scf*-GFP mice and administered tamoxifen at P2 to induce recombination (see Table S2 for a description of the mouse alleles used in this study). The Nestin-creER transgene has a somewhat different expression pattern as compared to endogenous *Nestin*[12,45,46], but has been used as a marker of niche cells in some contexts[32,47,48]. We enzymatically dissociated an entire femur and tibia at P4 or P14 and examined the frequencies of cells that were Tomato$^+$ and/or *Scf*-GFP$^+$: 0.3 to 0.9% of enzymatically dissociated bone/bone marrow cells were Tomato$^+$ at P4 to P14 and 30 to 40% of these cells were *Scf*-GFP$^+$ (Figure S4A and S4C). These cells included a subset of endothelial cells and subsets of perisinusoidal and periarteriolar stromal cells (Figure S4F and S5G), consistent with published analyses of the *Nestin-CreER* recombination pattern in early postnatal bone marrow[33]. When we gated on all *Scf*-GFP$^+$ cells in these specimens only 20 to 29% were Tomato$^+$ (Figure S4B and S4D). This demonstrates that Nestin-CreER recombined in a minority of *Scf*-GFP expressing cells in the bone marrow.

To test if *Nestin*-expressing cells contributed to the maintenance of HSCs in early postnatal bone marrow, we generated *Nestin-creER*; $Scf^{GFP/fl}$ mice and compared HSC frequency and hematopoiesis in these mice to $Scf^{GFP/fl}$ littermate controls. We treated the mice with tamoxifen at P2 and analyzed the bone marrow at P14. We observed no significant differences among *Nestin-creER*; $Scf^{GFP/fl}$ mice and littermate controls in bone marrow cellularity (Figure S4H), or in the frequencies of HSCs (Figure S4I), multipotent progenitor cells (MPPs; Figure S4J), hematopoietic progenitor cells (HPCs, Figure S4K), Lineage$^-$c-kit$^+$ (LK) myeloid progenitors (Figure S4L), common myeloid progenitors (CMPs), megakaryocyte-erythroid progenitors (MEPs), or granulocyte-macrophage progenitors (GMPs) (Figure S4M) and colony-forming units-erythroid (CFU-E) (Figure S4N) (see Table S3 for the surface markers used to isolate each cell population analyzed in this study). We also observed no difference in the reconstituting potential of bone marrow cells from *Nestin-creER*; $Scf^{GFP/fl}$ versus littermate control mice upon competitive transplantation into irradiated mice (Figure S4O).

We also treated *Nestin-creER; Ai47*-GFP (a conditional reporter) with tamoxifen at P2 and aged them to 8 weeks. Consistent with published studies that showed that cells recombined by Nestin-creER were extraordinarily rare in adult bone marrow and not a significant source of SCF or Cxcl12 for HSC maintenance or hematopoiesis[12,15], we found that the progeny

of Nestin-creER-expressing cells accounted for less than 0.007% of adult bone marrow cells (Figure S4E). These cells included small subsets of endothelial cells and CD140a/b$^+$ stromal cells (Figure S4E) that were orders of magnitude less frequent than SCF-expressing cells. We also observed no differences in bone marrow cellularity (Figure S4P) or in the frequencies of bone marrow HSCs, MPPs, HPCs, LK cells, CMPs, MEPs, GMPs, or CFU-Es (Figure S4Q–V) in *Nestin-cre*; *Scf*$^{GFP/fl}$ as compared to littermate control mice. HSCs and hematopoiesis, thus, did not depend upon SCF produced by cells that expressed Nestin-cre or Nestin-creER in early postnatal bone marrow.

NG2$^+$ cells are not a major source of SCF in early postnatal bone marrow

The scRNA-seq analysis suggested that *NG2*$^+$ cells were not one of the top sources of *Scf* or *Cxcl12* in early postnatal or adult bone marrow (Figure 2D and 2E). Comparison of *NG2* expression with *Scf* and *Cxcl12* expression across cell clusters showed limited overlap (Figure S3B–D). The only cell cluster that showed clear expression of both *NG2* and *Scf* was SMA$^+$ pericytes (Figure S3B and S3C). With respect to *Cxcl12*, multiple clusters of fibroblasts and SMA$^+$ pericytes expressed *NG2* and low levels of *Cxcl12* (Figure S3B and S3D).

We generated *NG2-cre*; *tdTomato*; *Scf*-GFP mice and analyzed Tomato and *Scf*-GFP expression in the bone marrow at P4, P14 and at 5 weeks of age. NG2-cre recombined in 94% of NG2$^+$ cells in P14 bone marrow (Figure S5G). Overall, 1.3% to 4.6% of enzymatically dissociated bone/bone marrow cells were Tomato$^+$ at P4, P14 and 5 weeks of age, and 51% to 68% of these cells were *Scf*-GFP$^+$ (Figure S5A, S5C and S5E). When we gated on all *Scf*-GFP$^+$ cells in these specimens, 88% to 98% were Tomato$^+$ (Figure S5B, S5D and S5F). Imaging and flow cytometric analysis showed that perisinusoidal stromal cells were Tomato$^+$ throughout the bone marrow (Figure S5I), including 98% of LepR$^+$ cells (Figure S5H). This was expected as chondrocytes and perichondrial cells express *NG2* (Figure 1G and ref[49]); therefore, the cells that give rise to LepR$^+$ cells[28,29] recombined with NG2-cre[31], though the *Lepr*$^+$ cells themselves exhibited little or no ongoing *NG2* expression (Figure S3B).

To test if *NG2*-expressing cells contributed to the maintenance of HSCs in early postnatal bone marrow, we generated *NG2-cre; Scf*$^{GFP/fl}$ mice and compared the bone marrow of these mice to *Scf*$^{GFP/fl}$ littermate controls at P14. The *NG2-cre; Scf*$^{GFP/fl}$ mice exhibited decreases in bone marrow cellularity (Figure S5J) and the frequencies of HSCs (Figure S5K), MPPs (Figure S5L), and CFU-Es (Figure S5P) but normal frequencies of HPCs (Figure S5M), LK myeloid progenitors (Figure S5N), and CMPs, MEPs, and GMPs (Figure S5O). Consistent with this, bone marrow cells from *NG2-cre*; *Scf*$^{GFP/fl}$ mice exhibited significantly reduced reconstituting potential as compared to control bone marrow cells upon competitive transplantation into irradiated mice (Figure S5Q). The depletion of HSCs and primitive hematopoietic progenitors likely reflected the deletion of *Scf* from LepR$^+$ cells and from a subset of endothelial cells in these mice[31].

Since the NG2-cre recombination pattern in the bone marrow did not reflect ongoing NG2 expression, we also tested if NG2$^+$ cells contributed to the early postnatal bone marrow niche by generating *NG2-creER*; *tdTomato*; *Scf*-GFP mice. We administered tamoxifen

at P2 to induce recombination. At P14, 0.12% of bone/bone marrow cells were Tomato$^+$ and 33% of these cells were *Scf*-GFP$^+$ (Figure S6A); however, when we gated on all *Scf*-GFP$^+$ cells, only 8.6% were Tomato$^+$ (Figure S6B). These Tomato$^+$ cells included rare perisinusoidal stromal cells with a position and morphology suggesting that they represented a small subset of LepR$^+$ cells (Figure S6C). Tomato$^+$ cells were more common in the metaphysis and epiphysis, where they were present in the growth plate and near growing bone surfaces where chondrocytes give rise to osteoblasts (Figure S6D). This suggests that many of the NG2$^+$ cells in the chondrocyte and fibroblast cell clusters (Figure 1G) were in the epiphysis/metaphysis.

We performed a similar analysis on 8 week-old *NG2-creER*; *tdTomato*; *Scf*-GFP mice. We found that only 0.0028% of bone marrow cells were Tomato$^+$ (Figure S6E) and only 0.17% of *Scf*-GFP$^+$ bone marrow cells were Tomato$^+$ (Figure S6F).

To test the function of NG2-creER$^+$ cells in early postnatal bone marrow, we generated *NG2-creER*; $Scf^{GFP/fl}$ and $Scf^{GFP/fl}$ littermate controls, treated them with tamoxifen at P2 and analyzed the bone marrow at P14. We observed no significant differences among *NG2-creER*; $Scf^{GFP/fl}$ and littermate control mice in bone marrow cellularity (Figure S6G), or in the frequencies of HSCs (Figure S6H), MPPs (Figure S6I), LK myeloid progenitors (Figure S6K), CMPs, MEPs, or GMPs (Figure S6L) or CFU-Es (Figure S6M). We observed no difference in the reconstituting potential of bone marrow cells from *NG2-creER*; $Scf^{GFP/fl}$ versus littermate control mice upon competitive transplantation into irradiated mice (Figure S6N). *NG2-creER*; $Scf^{GFP/fl}$ mice did have significantly lower frequencies of HPCs as compared to littermate controls (Figure S6J), though we did not detect any effect on other restricted progenitors or differentiated cells. Given the *NG2* and *Scf* expression by SMA$^+$ pericytes (Figure S3B and Figure 2D), it is possible that SMA$^+$ pericytes promote the maintenance of a subset of HPCs.

SCF from LepR$^+$ cells promotes myelopoiesis and erythropoiesis in postnatal marrow

The scRNA-seq analysis showed that LepR$^+$ stromal cells had the highest levels of *Scf* and *Cxcl12* expression in P4, P14, and 8 week-old bone marrow (Figure 2B–E). To further assess this, we analyzed *Scf*-GFP expression by non-hematopoietic and non-endothelial bone marrow stromal cells from femurs and tibias at P4 and P14. At P4, 45% of *Scf*-GFP$^+$ bone marrow stromal cells stained positively for anti-LepR antibody (Figures 3A) and 46% of LepR$^+$ cells were *Scf*-GFP$^+$ (Figure 3B). At P14, 98% of *Scf*-GFP$^+$ cells were LepR$^+$ (Figures 3C) and 54% of LepR$^+$ cells were *Scf*-GFP$^+$ (Figure 3D). Confocal imaging of femurs at P14 showed that nearly all LepR$^+$ cells in the diaphysis bone marrow were *Scf*-GFP$^+$ and that most cells that expressed high levels of *Scf*-GFP were LepR$^+$ (Figure 3E). LepR$^+$ cells were thus a major source of SCF in early postnatal bone marrow.

To test the functional importance of *Scf* produced by LepR$^+$ cells, we first analyzed the recombination efficiency of $Lepr^{cre}$ in early postnatal bone marrow. LepR antibody staining of dissociated cells from $Lepr^{cre}$; *tdTomato*; *Scf*-GFP bone marrow showed that $Lepr^{cre}$ recombined in only 10% of LepR$^+$ cells at P4 and 30% of LepR$^+$ cells at P14 (Figure S6O). The low recombination efficiency of $Lepr^{cre}$ in early postnatal bone marrow precluded the

use of this Cre allele to analyze the functional contribution of these cells to early postnatal hematopoiesis.

As an alternative approach, we used *Prx1-cre*, which recombines in limb mesenchyme, including LepR$^+$ cells, osteogenic progenitors, and osteoblasts, but not endothelial cells [16,50]. Since LepR negative osteolineage cells (cluster 1) and osteoblasts (cluster 2) do not express *Scf* (Figure 2A–D; Figure S3C), this approach allowed us to assess the functional importance of SCF made by LepR$^+$ cells in limb bone marrow. In bone marrow from the femurs and tibias of *Prx1-cre; tdTomato* mice, 93% of LepR$^+$ cells were Tomato$^+$, demonstrating high recombination efficiency (Figure 3F). We observed no significant differences among *Prx1-cre; Scf$^{fl/fl}$* mice and littermate controls in terms of bone marrow cellularity (Figure 3G) or the frequencies of HSCs (Figure 3H), MPPs (Figure 3I), HPCs (Figure 3J), CMPs or GMPs (Figure 3L) in the bone marrow. However, *Prx1-cre; Scf$^{fl/fl}$* mice had significantly lower frequencies of Lineage$^-$c-kit$^+$ (LK) myeloid progenitors (Figure 3K), MEPs (Figure 3L), CFU-Es (Figure 3M), Mac-1$^+$Gr-1$^+$ myeloid cells (Figure 3N), and Ter119$^+$ erythroid cells (Figure 3O). Conversely, the frequencies of B220$^+$ B cells and CD3$^+$ T cells increased in the bone marrow of *Prx1-cre; Scf$^{fl/fl}$* mice as compared to controls (Figure 3P). SCF made by *Prx1*-expressing mesenchymal cells was thus necessary for normal myelopoiesis and erythropoiesis in early postnatal bone marrow and the *Scf* made by *Prx1*-expressing cells came overwhelmingly from LepR$^+$ cells based on scRNA-seq analysis.

We observed no significant difference in the reconstituting activity of bone marrow cells from P14 *Prx1-cre; Scf$^{fl/fl}$* as compared to littermate control mice upon competitive transplantation into irradiated mice (Figure 3Q), consistent with their normal HSC frequency (Figure 3H). This suggests that SCF from LepR$^+$ cells is not required for HSC maintenance in early postnatal bone marrow. However, Prx1-cre recombines in limb mesenchyme but not in the axial skeleton. Therefore, it is possible that the functional importance of Prx1$^+$/LepR$^+$ cells was underestimated in these experiments if HSCs and other hematopoietic cells from the axial skeleton migrated to limb bones to compensate for the depletion of progenitors in limb bones.

SCF from endothelial cells promotes HSC maintenance in early postnatal bone marrow

By scRNA-seq, arteriolar endothelial cells at P4 and P14, and sinusoidal endothelial cells at P4, expressed higher levels of *Scf* as compared to the same cells at 8 weeks of age (Figure 2D). We confirmed this by quantitative reverse-transcription PCR (Figure 4A). At P4, 54% of bone marrow endothelial cells were *Scf*-GFP$^+$ (Figure 4B) and 25% of all *Scf*-GFP$^+$ cells in the bone marrow were CD31$^+$ endothelial cells (Figure 4C). At P14, 52% of bone marrow endothelial cells were *Scf*-GFP$^+$ (Figure 4D) and 49% all *Scf*-GFP$^+$ cells in the bone marrow were CD31$^+$ endothelial cells (Figure 4E). Confocal imaging showed *Scf*-GFP expression by arteriolar (Figure S6Q) and sinusoidal endothelial cells (Figure S6R) at P14.

To test the functional importance of SCF made by endothelial cells in early postnatal bone marrow, we compared *Tie2-cre; Scf $^{fl/fl}$* and littermate control mice. Although *Tie2-cre* also recombines in hematopoietic cells, CD45$^+$ and/or Ter119$^+$ hematopoietic cells do not express *Scf* in the bone marrow (Figure S6P)[12]. At P14, we observed no significant

differences between *Tie2-cre; Scf* $^{fl/fl}$ and littermate control mice in terms of bone marrow cellularity (Figure 4F) or the frequencies of MPPs (Figure 4H), HPCs (Figure 4I), LKs (Figure 4J), CMPs, MEPs, GMPs (Figure 4K), CFU-Es (Figure 4L), Mac-1^{+}Gr-1^{+} myeloid cells (Figure 4M), Ter119^{+} erythroid cells (Figure 4N), B220^{+} B cells or CD3^{+} T cells (Figure 4O). However, we did observe a significantly lower frequency of HSCs in the bone marrow of *Tie2-cre; Scf* $^{fl/fl}$ as compared to littermate control mice (Figure 4G). Consistent with this, bone marrow cells from P14 *Tie2-cre; Scf* $^{fl/fl}$ mice gave lower levels of donor cell reconstitution in all lineages as compared to control bone marrow cells upon competitive transplantation into irradiated mice (Figure 4P). SCF made by endothelial cells is thus necessary for the maintenance of normal numbers of HSCs, but not restricted hematopoietic progenitors, in early postnatal bone marrow. Homeostatic mechanisms in the bone marrow can generate normal numbers of restricted progenitors despite HSC depletion[51].

SCF is produced in membrane bound and secreted forms [52]. There is evidence that the membrane bound form is functionally important for the creation of hematopoietic stem/progenitor cell niches [52–54], though it is difficult to dissect the relative contributions of the two forms of SCF given the limited tools available to independently delete each form. We tested if membrane bound SCF contributed to the ability of endothelial cells to maintain HSCs in early postnatal bone marrow by generating *Tie2-cre*; *Scf-Ex7* $^{fl/fl}$ mice in which the transmembrane domain of SCF was deleted from endothelial cells [54]. Consistent with the results from *Tie2-cre; Scf* $^{fl/fl}$ mice, *Tie2-cre*; *Scf-Ex7* $^{fl/fl}$ mice also exhibited a significant reduction in the frequency of HSCs (Figure 4R) and the reconstituting activity of bone marrow cells upon competitive transplantation into irradiated mice (Figure 4Z') relative to bone marrow cells from littermate control mice. We did not detect any differences between *Tie2-cre*; *Scf-Ex7* $^{fl/fl}$ and littermate control mice in overall bone marrow cellularity (Figure 4Q), or in the frequencies of MPPs, HPCs, LKs, CMPs, MEPs, GMPs, CFU-Es, Mac-1^{+}Gr-1^{+} myeloid cells, Ter119^{+} erythroid cells, B220^{+} B cells or CD3^{+} T cells (Figure 4S–Z). Membrane bound SCF from endothelial cells thus appears to contribute to HSC maintenance in early postnatal bone marrow.

HSCs localize to sinusoids in early postnatal bone marrow

We assessed the localization of HSCs in P4 and P14 bone marrow by performing deep confocal imaging of half bones from *α-catulin*$^{GFP/+}$ mice[8]. *α-catulin*-GFP^{+}c-kit^{+} bone marrow cells are highly enriched for long-term multilineage reconstituting HSCs[8]. At P14, 0.023% of whole bone marrow cells were *α-catulin*-GFP^{+}c-kit^{+} and 64% of *α-catulin*-GFP^{+}c-kit^{+} bone marrow cells were CD150^{+}CD48^{-}Lineage^{-} (Figure S7A). 54% of CD150+CD48^{-}Lineage^{-} bone marrow cells were *α-catulin*-GFP^{+}c-kit^{+} (Figure S7B). At P4, 80% of HSCs were closer to sinusoidal blood vessels than to arterioles, transition zone vessels, or bone surfaces (Figure S7C and 5D). 70% of HSCs were within 10 μm of sinusoidal blood vessels, significantly more than would be expected by chance based on the distribution of random spots in the bone marrow (Figure S7E). Another 17% of HSCs were within 10 μm of transition zone vessels, which have properties that are intermediate between sinusoids and arterioles (Figure S7E). Only around 7% of HSCs were within 10 μm of arterioles and 3% were within 10 μm of bone surfaces (Figure S7E). At P14, 88% of HSCs were closer to sinusoidal blood vessels than to arterioles, transition zone vessels, or

bone surfaces. This is more than would be expected by chance based on the distribution of random spots (Figure S7F and 7G). At P14, 64% of HSCs were within 10 μm of sinusoidal blood vessels, (Figure S7H). Most HSCs in early postnatal bone marrow thus localized adjacent to sinusoidal blood vessels, as we have reported in adult bone marrow[5,8].

DISCUSSION

We observed extensive remodeling of the bone marrow stroma between P4 and 8 weeks of age. LepR$^+$ cells, LepR$^+$Oln$^+$ cells, arteriolar endothelial cells, and sinusoidal endothelial cells all increased in frequency during this period while the frequencies of some other stromal cell populations declined (Table S1). The properties of these cell populations also changed over time (Figure 2F–H). During the transition into adulthood LepR$^+$ cells increased their expression of many secreted factors that regulate hematopoiesis and bone marrow inflammation as well as their expression of antigen presentation genes.

Similar to adult bone marrow, LepR$^+$ cells and endothelial cells expressed the highest levels of *Scf* in early postnatal bone marrow (Figure 2D). LepR$^+$ cells also expressed the highest levels of *Cxcl12* (Figure 2E). In early postnatal bone marrow, *Scf* from endothelial cells was necessary for the maintenance of normal numbers of HSCs (Figure 4), while *Scf* from LepR$^+$/Prx1$^+$ cells was necessary for the maintenance of normal numbers of myeloid and erythroid progenitors (Figure 3). Indeed, endothelial cells expressed higher levels of *Scf* at P4 and P14 than in 8 week-old bone marrow (Figure 4A). Among endothelial cells, *Scf* is expressed mainly by arteriolar endothelial cells in adult bone marrow [13,20,21,55] but at P4 we found it was also expressed by sinusoidal endothelial cells (Figure 2D). Endothelial cells thus play an important role in promoting the maintenance of normal numbers of HSCs in neonatal bone marrow. Arteriolar endothelial cells also regulate the initial engraftment of hematopoietic stem/progenitor cells in fetal bone marrow by secreting Wnts [55].

While LepR$^+$ cells are an important source of SCF for the maintenance of HSCs and restricted hematopoietic progenitors in adult bone marrow [12,51,56] these cells did not seem necessary for HSC maintenance in early postnatal bone marrow (Figure 3H and 3Q). It is possible that *Scf* was most highly expressed by LepR$^+$ cells (Figure 2D) but dispensable for HSC maintenance in early postnatal bone marrow because LepR$^+$ cells were rare in early postnatal bone marrow, becoming much more abundant in the weeks after birth (Figure 1E).

Deletion of membrane bound SCF from endothelial cells (Figure 4R and 4Z') phenocopied the HSC depletion observed after deletion of all SCF from endothelial cells (Figure 4G and 4P). This suggests that membrane bound SCF from endothelial cells promotes HSC maintenance in early postnatal bone marrow. Nonetheless, it remains possible that soluble SCF produced by endothelial cells and/or LepR$^+$ cells contributes to the effects of these cells on the maintenance of HSCs and/or restricted hematopoietic progenitors in the bone marrow.

Limitations of our study

It remains possible that there are cells other than endothelial cells and LepR$^+$/Prx1$^+$ cells that functionally contribute to the synthesis of SCF in early postnatal bone marrow, even though other cell types expressed lower levels of SCF. It is likely that other cells contribute

to the regulation of early postnatal bone marrow niches through the synthesis of other factors.

METHODS

RESOURCE AVAILABILITY

Lead contact and materials availability—Further information and requests for resources and reagents should be directed to and will be fulfilled by the Lead Contact, Sean Morrison (sean.morrison@utsouthwestern.edu).

Data and code availability—The single cell RNA sequencing data generated in this paper have been deposited at SRA (BioProject ID: PRJNA835050). Accession numbers are listed in the key resources table. Source code related to the analysis of these data can be found at https://git.biohpc.swmed.edu/CRI/morrison-lab/scRNASeq. Any additional information required to reanalyze the data reported in this paper is available from the Lead Contact upon request.

EXPERIMENTAL MODEL AND SUBJECT DETAILS

Mice—Table S2 provides a description of each of the mouse alleles used in this study. *Scf*^{GFP} (*Kitl*$^{tm1.1Sjm}$; a GFP knockin allele that reports *Scf* expression), *Scf* ^{fl} (*Kitl*$^{tm2.1Sjm}$; a floxed allele for deletion of *Scf*) and *α-catulin*^{GFP} (*Ctnnal1*$^{tm1.1Sjm}$; a GFP knockin allele that reports *α-catulin* expression) were generated in our laboratory[8,12]. *Tie2-cre* (B6.Cg-Tg(Tek-cre)1Ywa; a Cre allele expressed by endothelial and hematopoietic cells)[58], *Prx1-cre* (B6.Cg-Tg(Prrx1-cre)1Cjt; a Cre allele expressed by limb mesenchymal cells)[50], *Lepr*^{cre} (B6.129(Cg)-Lepr$^{tm2(cre)Rck}$; a Cre allele expressed by *Lepr*$^{+}$ cells)[38], *Nestin-cre* (B6.Cg-Tg(Nes-cre)1Kln; a Cre allele expressed by *Nestin*$^{+}$ cells), *Ng2-creER* (B6.Cg-Tg(Cspg4-cre/Esr1)BAkik; a CreER allele expressed by *NG2*$^{+}$ cells), *NG2-cre* (B6; FVB-*Ifi208*$^{Tg(Cspg4-cre)1Akik}$; a Cre allele expressed by *NG2*$^{+}$ cells)[59] and *Rosa26-CAG-loxp-stop-loxp-tdTomato* (tdTomato) (B6.Cg-Gt(ROSA)26Sor$^{tm9(CAG-Rosa26-tdTomato)Hze}$; a Tomato reporter that is induced by Cre-mediated recombination) mice were obtained from Jackson Laboratory. *Rosa26-CAG-loxp-stop-loxp-eGFP* (Ai47-GFP; a GFP reporter that is induced by Cre-mediated recombination) mice were obtained from Hongkui Zeng[60]. *Nestin-creER* mice (a CreER allele expressed by *Nestin*$^{+}$ cells) were obtained from G. Fishell[61]. *Kitl*$^{LEx7/Lex7}$ mice *(Scf-Ex7*$^{fl/fl}$; this allows the membrane bound form of *Scf* to be deleted by Cre-mediated recombination) were obtained from Claus Nerlov and Sten Eirik Jacobsen[54]. All mice were backcrossed at least six times onto a C57BL/Ka background. To induce Cre-mediated recombination in *Nestin-creER* and *NG2-creER* mice, the mice were given an intraperitoneal injection of 50μg of tamoxifen dissolved in corn oil at P2. C57BL/Ka-Thy-1.2 (CD45.1) and C57BL/Ka-Thy-1.1/Thy-1.2 (CD45.1/C45.2) mice were used as recipient mice and a source of competitive whole bone marrow cells in transplantation experiments. Recipient mice were given Baytril (0.1 mg/ml in the drinking water) for 1 week prior to, and one month after, irradiation. All mice were housed in AAALAC-accredited, specific-pathogen-free animal care facilities at the University of Texas Southwestern Medical Center (UTSW). Mice were housed under a 12h:12h light:dark cycle with a temperature of 18–24°C and humidity of 35–60% and were fed Teklad Global 16%

Protein Rodent Diet ad libitum. All procedures were approved by the UTSW Institutional Animal Care and Use Committee.

METHOD DETAILS

Flow cytometric analysis of hematopoietic cells—Tibias and femurs were crushed, triturated, and resuspended in staining medium (Ca^{2+} and Mg^{2+} free Hank's buffered salt solution (HBSS) supplemented with 2% heat inactivated bovine serum) and filtered through a 40 μm cell strainer to generate a single cell suspension. Cells were counted, and then stained with antibodies at 4°C for 30 minutes (except for anti-CD34 that was incubated for 90 minutes). For staining of HSCs, MPPs and HPCs, cells were stained with fluorophore-conjugated antibodies against c-kit, Sca1, CD150, CD48 and lineage markers (CD2, CD3, CD5, CD8a, B220, Ter119, and Gr-1). For staining of restricted hematopoietic and erythroid progenitors, cells were first stained with biotin-conjugated anti-CD34 antibody, washed with staining medium and then resuspended in fluorophore-conjugated antibodies against c-kit, Sca1, CD150, CD48, CD105, CD41, as well as BV510-conjugated streptavidin and fluorophore-conjugated antibodies against lineage markers (CD2, CD3, CD5, CD8a, B220, Ter119, and Gr-1). For analysis of lymphoid and myeloid cells, cells were stained with fluorophore-conjugated antibodies against B220, CD3, Gr-1, Mac1, Ter119. After staining with antibodies, the cells were washed and resuspended in staining medium with 0.2μg/ml of propidium iodide to exclude dead cells. The cells were then analyzed using a FACS Canto cytometer. Markers for each hematopoietic cell population are listed in Table S2.

Flow cytometry analysis and sorting of stromal cells—To isolate bone marrow stromal cells, whole tibias and femurs were placed in enzymatic dissociation buffer (HBSS with Ca^{2+} and Mg^{2+}, supplemented with DNase I (200U/ml) and Liberase^{DL} (250mg/ml)), minced with scissors, and then dissociated by agitating for 30 minutes at 37°C. Bone marrow fragments were allowed to sediment for ~1 min, then the cell suspension was collected and the enzymes were quenched by adding staining medium with 7 mM EDTA. Cells were washed once in staining medium and incubated with biotin-conjugated goat anti-LepR antibody for 90 min at 4°C. Cells were washed and then incubated with fluorophore-conjugated antibodies against CD45, Ter119, CD31 and BV421-conjugated streptavidin. For endothelial cell analyses in neonatal mice, the cells were stained with anti-VE-cadherin or anti-CD31 antibody. Dead cells and debris were excluded by gating on forward scatter, side scatter, and the viability dye Ghost dye Red 780. Samples were analyzed and cells were isolated (with two successive rounds of sorting to ensure high purity) using a FACS Aria II flow cytometer.

RNA extraction and real time quantitative PCR—5,000–10,000 cells were sorted into staining medium, pelleted by centrifugation, and resuspended in Trizol. RNA was extracted and reverse transcribed into cDNA using iScript Reverse Transcription Supermix for RT-qPCR. Primers used for qPCR are listed in Table S3. Transcript levels were normalized to *Actin (Actb)* and fold change was calculated based on ΔCt.

BrdU incorporation—To assess the rate of 5-Bromo-2'-deoxyuridine (BrdU) incorporation into dividing cells, mice were given an intraperitoneal injection of 0.1 mg

BrdU per g of body mass in PBS. Two hours later, the frequency of $BrdU^+$ cells was analyzed by flow cytometry using the APC BrdU Flow Kit (BD Biosciences).

Single cell RNA sequencing—Whole tibias and femurs were dissociated as described above. Cells were stained with antibodies against CD45, CD71, CD2, CD3, CD5, CD8, CD11b, Ter-119, B220 and Gr-1. Dead cells and debris were excluded by gating on forward scatter, side scatter, and the viability dye 4′,6-diamidino-2-phenylindole (DAPI; 2 μg/ml). Bone marrow stromal cells were isolated by sorting live cells that were negative for hematopoietic markers. 15,000 cells were sorted into staining medium, then pelleted by centrifugation and resuspended in 40 μl of staining medium. Single cell RNA sequencing libraries were generated using Chromium Next GEM Single Cell 3' Reagent Kits v3.1 (10xGenomics) according to the manufacturer's instructions. Briefly, cells, reagents (10xGenomics, PN-1000130), gel beads (10xGenomics, 2000164), and partitioning oil (10xGenomics, 220088) were loaded into the Chromium Next GEM Chip G (10xGenomics, 200177). The chip was loaded into the Chromium Controller (10xGenomics) to generate Gel Bead-In-Emulsions (GEMs). After reverse transcription using the GEM-RT incubation protocol, GEMs were broken with recovery reagent (10xGenomics, 220016), cDNA was purified with DynaBeads MyOne Silane beads (10xGenomics, 2000048), amplified by PCR for 12 cycles, and further purified with SPRIselect reagent (Beckman Coulter, B23318). The DNA concentration and amplicon size were measured using a Tapestation (Agilent) with D1000 high sensitivity screentapes (Agilent, 5067–5582), and cDNA yield was measured using the Qubit DNA high sensitivity assay (Invitrogen, Q32854), to ensure the amplified cDNA met quality control standards. After fragmentation, end-repair, A-tailing and size selection, cDNA was ligated with adaptor and purified with SPRIselect reagents, according to 10xGenomics instructions. Libraries were amplified by PCR with sample index primers from the Chromium i7 Multiplex kit (10xGenomics, PN-120262), typically for a total of 14 cycles, depending on the original cDNA yield measured by Qubit. Final PCR products were subjected to double-sided size selection with SPRIselect reagents to eliminate fragments larger and smaller than the target amplicons. Library cDNA concentration and size were determined using the Agilent Tapestation with D1000 screentapes (Agilent, 5067–5582), as well as the Qubit DNA high sensitivity assay. cDNA libraries were sequenced using a NextSeq 500 sequencer using the 150bp high output sequencing kit (Illumina), with the following pair-end sequencing settings: Read 1 – 28bp, i7 index – 8bp, Read 2 – 122bp, generating ~400 million raw reads per run.

Single cell RNA sequencing data analysis—Cell Ranger single cell software suite (version 4.0, https://support.10xgenomics.com/single-cell-gene-expression/software/pipelines/4.0/what-is-cell-ranger) was used to perform sample demultiplexing, alignment, filtering, and UMI counting. In total, we analyzed 15,189 cells from P4 mice with 41,486 reads per cell and 90.9% of the reads were uniquely mapped to Cell Ranger's mouse reference genome mm10-2020-A. The median UMIs and genes per cell for the P4 specimens were 6,864 and 2,392, respectively. We sequenced 13,206 cells with 43,679 reads per cell from P14 specimens and 91.1% of the reads were uniquely mapped to the mouse reference genome. The median UMIs and genes per cell for P14 specimens were 7,896 and 2,720, respectively. We sequenced 11,893 cells with 70,245 reads per cell from adult bone

marrow and 88.8% of reads uniquely mapped to the mouse reference genome. The median UMIs and genes per cell for the adult bone marrow were 5,110 and 1,715, respectively. The numbers and distribution of detected genes per cell were comparable across samples.

Cell quality filtering, normalization, sample integration, clustering, gene expression, and data visualization were analyzed with the Seurat package (version 3.2.3) [62] on R (version 4.0.2). Cells were first filtered to have 100 to 10,000 detected genes, 100 to 100,000 UMI counts, and less than 5% of total UMIs mapping to the mitochondrial genome. After quality filtering and removing unwanted cells from the dataset, we applied Seurat's SCTransform on the UMI counts to account for the variability among cells caused by different sequencing depths and potential batch effects. We avoided clustering cells based on differences in cell cycle status or transcription of mitochondrial genes by subtracting such differences from the data used for clustering. The 3,000 most variable genes across the transformed cells were selected using SelectIntegrationFeatures, and samples were integrated using those genes with an anchor set of cells found by FindIntegrationAnchors. Integrated data were reduced to 30 dimensions by RunPCA. Dimension-reduced cells were clustered by FindNeighbors followed by FindClusters, and UMAP plots were generated by RunUMAP using the integrated, dimension-reduced cells. For the gene expression analyses, we normalized the UMI count data by the total UMIs per cell, multiplied by a scale factor of 10,000 and log-transformed (log1p) the result. Normalized data were used for gene-expression visualizations. Heatmaps were based on the z-scores of normalized and log-transformed UMI counts.

We identified 33 clusters, with 17 of them expressing hematopoietic cell markers, likely representing contaminating hematopoietic cells. These hematopoietic clusters were removed and the remaining 16 clusters of non-hematopoietic stromal cells were analyzed further.

Analysis of differential gene expression among cell clusters was performed using the FindAllMarkers function, and differential gene expression between two groups of cells was performed using the FindMarkers function with the Wilcoxon rank sum test. Markers that were used to identify and discriminate cell clusters were selected for having $p<0.01$ for pairwise comparisons among clusters, expression by >10% cells in a cluster, and fold change >1.28 between clusters. Violin plots, heatmaps, and individual UMAP plots for genes were generated using Seurat's VlnPlot, DoHeatmap, and FeaturePlot functions, respectively.

Pseudotime trajectory analysis—*Lepr*$^+$ cells, *Lepr*$^+$*Osteolectin*$^+$ cells, Osteolineage cells, Osteoblasts, Chondro-1, Chondro-2, Chondro-3, and Chondro-4 cells were selected from Seurat-integrated samples for the single-cell trajectory analysis. Chondro-1 was specified as the initial cell cluster, though the trajectory analysis showed that *Lepr*$^+$ cells and other osteolineage cells arose from multiple distinct chondrocyte cell clusters. Cells from all time points were analyzed together as well as separately at P4, P14, and 8 weeks. The analysis was performed using Monocle 3[63].

Gene ontology enrichment analysis—*Lepr*$^+$ cells at P4 and 8 weeks of age were selected from Seurat-integrated samples for the Gene Ontology (GO) enrichment analysis. Genes that were significantly differentially expressed between *Lepr*$^+$ cells at these time

points were identified and enriched gene sets were determined with adjusted $p<0.05$. The top 20 enriched gene sets for each timepoint were visualized by the R package clusterProfiler 3.18.1[64].

Bone marrow reconstitution assays—Recipient (CD45.1/CD45.2) mice were irradiated using an XRAD 320 X-ray irradiator (Precision X-Ray Inc.) with two doses of 540 rad at least 4h apart. For whole bone marrow transplantation, 300,000 unfractionated bone marrow cells from donor (CD45.2) and competitor (CD45.1) mice were mixed and injected intravenously through the retro-orbital venous sinus. Every 4 weeks until at least 16 weeks after transplantation, blood was collected from the submandibular vein and subjected to ammonium-chloride potassium chloride red cell lysis. Cells were then stained with antibodies against CD45.1, CD45.2, Mac-1, Gr-1, B220, and CD3 to evaluate levels of donor cell engraftment in the myeloid, B, and T cell lineages.

Deep imaging of HSC localization in half bones—Sample preparation and immunostaining of bisected (half) femurs were performed as previously described[8]. Freshly dissected femurs from *α-catulin*-GFP mice were cleared, stained, and imaged. Briefly, femurs were fixed in 4% paraformaldehyde solution in PBS for 6 hours with gentle rocking at 4°C. After fixation, the bones were embedded in OCT embedding medium. Each femur was trimmed to a half bone using a cryostat and then washed three times in PBS. Non-specific antibody binding was blocked by incubating half bones in whole mount staining medium (PBS with 5% donkey serum, 0.5% IgePal630, and 10% DMSO) overnight at room temperature. Half bones were then stained in whole mount staining medium with primary antibodies against CD105, laminin, GFP, DsRed/Tomato, and c-kit for three days at room temperature. The samples were washed three times for 5 minutes in PBS and then overnight in PBS. Half bones were then stained with secondary antibodies (Alexa Fluor 647-AffiniPure F(ab′)2 Fragment Donkey Anti-Chicken IgY, Alexa Fluor 488-AffiniPure F(ab′)2 Fragment Donkey Anti-Rabbit IgG, and 555-conjugated donkey anti-goat antibodies) for three days at room temperature. The samples were washed three times for 5 minutes in PBS and then overnight in PBS. Bone clearing was performed in eppendorf tubes, gently rotating at room temperature, first by dehydrating through a methanol series, before clearing with Murray's clear (1:2 Benzyl Alcohol: Benzyl Benzoate; BABB) solution[8]. Half bones were mounted in BABB and three-dimensional images were acquired using a Leica SP8 confocal microscope.

We analyzed the images to assess the localization of *α-catulin*-GFP$^+$c-kit$^+$ cells relative to arterioles, sinusoids, transition zone vessels and bone surfaces in P4 and P14 bone marrow. Confocal tiled Z-stack images were reconstructed in 3 dimensions and analyzed using Andor Imaris 9.9 software. The bone was segmented manually based on morphology using the manual surface function. We distinguished blood vessels based on anatomical position, morphology and continuity of basal lamina, visualized using anti-Laminin and anti-CD105 antibody staining as detailed previously[8]. The vasculature was manually segmented based on distance to bone (transition vessels), or morphology (arterioles and sinusoids). Vessel iso-surfaces were created based on fluorescent signal intensity as detailed previously[8]. Individual *α-catulin*–GFP$^+$c-kit$^+$ cell were identified manually and labeled with digital

spots using the spots function. Random spots were generated as previously described[8]. We calculate the shortest distances of each *catulin*–GFP$^+$c-kit$^+$ cell and random spot to blood vessels and bone surfaces using spot to surface statistics in Andor Imaris image analysis software.

Quantification and statistical analysis

Data in all figures were obtained in at least three independent experiments using different mice, as indicated in each figure panel. Mice were allocated to experiments randomly and samples processed in an arbitrary order, but formal randomization techniques were not used. No formal blinding was applied when performing the experiments or analyzing the data. Samples sizes were not pre-determined based on statistical power calculations but were based on our experience with these assays. No data were excluded.

Prior to analyzing the statistical significance of differences among groups, we tested whether data were normally distributed and whether variance was similar among groups. To test for normality, we performed the Shapiro–Wilk tests when $3 \leq n < 20$ or D'Agostino Omnibus tests when $n \geq 20$. To test whether variability significantly differed among groups we performed *F*-tests (for experiments with two groups) or Levene's median tests (for experiments with more than two groups). When the data significantly deviated from normality or variability significantly differed among groups, we log2-transformed the data and tested again for normality and variability. If the transformed data no longer significantly deviated from normality and equal variability, we performed parametric tests on the transformed data. If log2-transformation was not possible or the transformed data still significantly deviated from normality or equal variability, we performed non-parametric tests on the non-transformed data.

When data or log2-transformed data were normal and equally variable, statistical analyses were performed using Student's t-tests (when there were two groups) or a one-way ANOVA (when there were more than two groups). When the data or log2-transformed data were normal but unequally variable, statistical analyses were performed using Welch's t-tests (when there were two groups). When the data and log2-transformed data were abnormal or unequally variable, statistical analysis was performed using Mann-Whitney (when there were two groups) or nparLD tests (when there were two groups measured at multiple time points). P-values from multiple comparisons were adjusted using Holm-Sidak's method after Student's t-tests or Mann-Whitney tests, Tukey's method after one-way ANOVA, or Benjiamini-Hochberg (FDR) method after nparLD tests. All statistical tests were two-sided. All data represent mean ± standard deviation. Statistical tests were performed using GraphPad Prism (9.1.0) or R (4.0.2). Flow cytometry data were analyzed using Flowjo v.10.4 (Flowjo, LLC).

Supplementary Material

Refer to Web version on PubMed Central for supplementary material.

ACKNOWLEDGMENTS

S.J.M. is a Howard Hughes Medical Institute (HHMI) Investigator, the Mary McDermott Cook Chair in Pediatric Genetics, the Kathryn and Gene Bishop Distinguished Chair in Pediatric Research, the director of the Hamon Laboratory for Stem Cells and Cancer, and a Cancer Prevention and Research Institute of Texas Scholar. This study was supported by funding from the National Institutes of Health (DK118745) and the Kleberg Foundation. M.M.M. was supported by a National Research Service Award from the NIH (F32 HL124947). We thank Claus Nerlov and Sten Eirik Jacobsen for kindly providing the *Kitl*$^{LEx7/Lex7}$ *(Scf-Ex7*$^{fl/fl}$*)* mice. We thank N. Loof, T. Shih, C. Cantu, G. Wilson and the Moody Foundation Flow Cytometry Facility as well as the BioHPC high performance computing cloud at the UT Southwestern Medical Center for providing computational resources for sequencing data storage and analyses. We thank the Integrated Microscopy and Imaging Laboratory at Texas A&M College of Medicine. Thanks to Claus Nerlov and Sten Eirik Jacobsen for providing the *Kitl*$^{LEx7/Lex7}$ mice *(Scf-Ex7*$^{fl/fl}$) that enabled deletion of the membrane bound form of *Scf* using Cre-mediated recombination.

INCLUSION AND DIVERSITY

We support inclusive, diverse, and equitable conduct of research

REFERENCES

1. Bertrand JY, Chi NC, Santoso B, Teng S, Stainier DY, and Traver D (2010). Haematopoietic stem cells derive directly from aortic endothelium during development. Nature 464, 108–111. 10.1038/nature08738. [PubMed: 20154733]
2. Boisset JC, van Cappellen W, Andrieu-Soler C, Galjart N, Dzierzak E, and Robin C (2010). In vivo imaging of haematopoietic cells emerging from the mouse aortic endothelium. Nature 464, 116–120. 10.1038/nature08764. [PubMed: 20154729]
3. Kissa K, and Herbomel P (2010). Blood stem cells emerge from aortic endothelium by a novel type of cell transition. Nature 464, 112–115. 10.1038/nature08761. [PubMed: 20154732]
4. Mikkola HK, and Orkin SH (2006). The journey of developing hematopoietic stem cells. Development 133, 3733–3744. 10.1242/dev.02568. [PubMed: 16968814]
5. Kiel MJ, Yilmaz OH, Iwashita T, Yilmaz OH, Terhorst C, and Morrison SJ (2005). SLAM family receptors distinguish hematopoietic stem and progenitor cells and reveal endothelial niches for stem cells. Cell 121, 1109–1121. 10.1016/j.cell.2005.05.026. [PubMed: 15989959]
6. Sugiyama T, Kohara H, Noda M, and Nagasawa T (2006). Maintenance of the hematopoietic stem cell pool by CXCL12-CXCR4 chemokine signaling in bone marrow stromal cell niches. Immunity 25, 977–988. 10.1016/j.immuni.2006.10.016. [PubMed: 17174120]
7. Nombela-Arrieta C, Pivarnik G, Winkel B, Canty KJ, Harley B, Mahoney JE, Park SY, Lu J, Protopopov A, and Silberstein LE (2013). Quantitative imaging of haematopoietic stem and progenitor cell localization and hypoxic status in the bone marrow microenvironment. Nat Cell Biol 15, 533–543. 10.1038/ncb2730. [PubMed: 23624405]
8. Acar M, Kocherlakota KS, Murphy MM, Peyer JG, Oguro H, Inra CN, Jaiyeola C, Zhao Z, Luby-Phelps K, and Morrison SJ (2015). Deep imaging of bone marrow shows non-dividing stem cells are mainly perisinusoidal. Nature 526, 126–130. 10.1038/nature15250. [PubMed: 26416744]
9. Chen JY, Miyanishi M, Wang SK, Yamazaki S, Sinha R, Kao KS, Seita J, Sahoo D, Nakauchi H, and Weissman IL (2016). Hoxb5 marks long-term haematopoietic stem cells and reveals a homogenous perivascular niche. Nature 530, 223–227. 10.1038/nature16943. [PubMed: 26863982]
10. Christodoulou C, Spencer JA, Yeh SA, Turcotte R, Kokkaliaris KD, Panero R, Ramos A, Guo G, Seyedhassantehrani N, Esipova TV, et al. (2020). Live-animal imaging of native haematopoietic stem and progenitor cells. Nature 578, 278–283. 10.1038/s41586-020-1971-z. [PubMed: 32025033]
11. Kokkaliaris KD, Kunz L, Cabezas-Wallscheid N, Christodoulou C, Renders S, Camargo F, Trumpp A, Scadden DT, and Schroeder T (2020). Adult blood stem cell localization reflects the abundance of reported bone marrow niche cell types and their combinations. Blood 136, 2296–2307. 10.1182/blood.2020006574. [PubMed: 32766876]

12. Ding L, Saunders TL, Enikolopov G, and Morrison SJ (2012). Endothelial and perivascular cells maintain haematopoietic stem cells. Nature 481, 457–462. 10.1038/nature10783. [PubMed: 22281595]

13. Xu C, Gao X, Wei Q, Nakahara F, Zimmerman SE, Mar J, and Frenette PS (2018). Stem cell factor is selectively secreted by arterial endothelial cells in bone marrow. Nat Commun 9, 2449. 10.1038/s41467-018-04726-3. [PubMed: 29934585]

14. Chen Q, Liu Y, Jeong HW, Stehling M, Dinh VV, Zhou B, and Adams RH (2019). Apelin(+) Endothelial Niche Cells Control Hematopoiesis and Mediate Vascular Regeneration after Myeloablative Injury. Cell Stem Cell 25, 768–783 e766. 10.1016/j.stem.2019.10.006. [PubMed: 31761723]

15. Ding L, and Morrison SJ (2013). Haematopoietic stem cells and early lymphoid progenitors occupy distinct bone marrow niches. Nature 495, 231–235. 10.1038/nature11885. [PubMed: 23434755]

16. Greenbaum A, Hsu YM, Day RB, Schuettpelz LG, Christopher MJ, Borgerding JN, Nagasawa T, and Link DC (2013). CXCL12 in early mesenchymal progenitors is required for haematopoietic stem-cell maintenance. Nature 495, 227–230. 10.1038/nature11926. [PubMed: 23434756]

17. Himburg HA, Termini CM, Schlussel L, Kan J, Li M, Zhao L, Fang T, Sasine JP, Chang VY, and Chute JP (2018). Distinct Bone Marrow Sources of Pleiotrophin Control Hematopoietic Stem Cell Maintenance and Regeneration. Cell Stem Cell 23, 370–381 e375. 10.1016/j.stem.2018.07.003. [PubMed: 30100167]

18. Zhou BO, Ding L, and Morrison SJ (2015). Hematopoietic stem and progenitor cells regulate the regeneration of their niche by secreting Angiopoietin-1. Elife 4, e05521. 10.7554/eLife.05521. [PubMed: 25821987]

19. Fang S, Chen S, Nurmi H, Leppanen VM, Jeltsch M, Scadden D, Silberstein L, Mikkola H, and Alitalo K (2020). VEGF-C protects the integrity of the bone marrow perivascular niche in mice. Blood 136, 1871–1883. 10.1182/blood.2020005699. [PubMed: 32842144]

20. Tikhonova AN, Dolgalev I, Hu H, Sivaraj KK, Hoxha E, Cuesta-Dominguez A, Pinho S, Akhmetzyanova I, Gao J, Witkowski M, et al. (2019). The bone marrow microenvironment at single-cell resolution. Nature 569, 222–228. 10.1038/s41586-019-1104-8. [PubMed: 30971824]

21. Baryawno N, Przybylski D, Kowalczyk MS, Kfoury Y, Severe N, Gustafsson K, Kokkaliaris KD, Mercier F, Tabaka M, Hofree M, et al. (2019). A Cellular Taxonomy of the Bone Marrow Stroma in Homeostasis and Leukemia. Cell 177, 1915–1932 e1916. 10.1016/j.cell.2019.04.040. [PubMed: 31130381]

22. Baccin C, Al-Sabah J, Velten L, Helbling PM, Grunschlager F, Hernandez-Malmierca P, Nombela-Arrieta C, Steinmetz LM, Trumpp A, and Haas S (2020). Combined single-cell and spatial transcriptomics reveal the molecular, cellular and spatial bone marrow niche organization. Nat Cell Biol 22, 38–48. 10.1038/s41556-019-0439-6. [PubMed: 31871321]

23. Zhong L, Yao L, Tower RJ, Wei Y, Miao Z, Park J, Shrestha R, Wang L, Yu W, Holdreith N, et al. (2020). Single cell transcriptomics identifies a unique adipose lineage cell population that regulates bone marrow environment. Elife 9. 10.7554/eLife.54695.

24. Matsushita Y, Nagata M, Kozloff KM, Welch JD, Mizuhashi K, Tokavanich N, Hallett SA, Link DC, Nagasawa T, Ono W, and Ono N (2020). A Wnt-mediated transformation of the bone marrow stromal cell identity orchestrates skeletal regeneration. Nat Commun 11, 332. 10.1038/s41467-019-14029-w. [PubMed: 31949165]

25. Zhou BO, Yue R, Murphy MM, Peyer JG, and Morrison SJ (2014). Leptin-receptor-expressing mesenchymal stromal cells represent the main source of bone formed by adult bone marrow. Cell Stem Cell 15, 154–168. 10.1016/j.stem.2014.06.008. [PubMed: 24953181]

26. Mizoguchi T, Pinho S, Ahmed J, Kunisaki Y, Hanoun M, Mendelson A, Ono N, Kronenberg HM, and Frenette PS (2014). Osterix marks distinct waves of primitive and definitive stromal progenitors during bone marrow development. Dev Cell 29, 340–349. 10.1016/j.devcel.2014.03.013. [PubMed: 24823377]

27. Pineault KM, Song JY, Kozloff KM, Lucas D, and Wellik DM (2019). Hox11 expressing regional skeletal stem cells are progenitors for osteoblasts, chondrocytes and adipocytes throughout life. Nat Commun 10, 3168. 10.1038/s41467-019-11100-4. [PubMed: 31320650]

28. Shu HS, Liu YL, Tang XT, Zhang XS, Zhou B, Zou W, and Zhou BO (2021). Tracing the skeletal progenitor transition during postnatal bone formation. Cell Stem Cell 28, 2122–2136 e2123. 10.1016/j.stem.2021.08.010. [PubMed: 34499868]
29. Matsushita Y, Chu AKY, Tsutsumi-Arai C, Orikasa S, Nagata M, Wong SY, Welch JD, Ono W, and Ono N (2022). The fate of early perichondrial cells in developing bones. Nat Commun 13, 7319. 10.1038/s41467-022-34804-6. [PubMed: 36443296]
30. Ono N, Ono W, Mizoguchi T, Nagasawa T, Frenette PS, and Kronenberg HM (2014). Vasculature-associated cells expressing nestin in developing bones encompass early cells in the osteoblast and endothelial lineage. Dev Cell 29, 330–339. 10.1016/j.devcel.2014.03.014. [PubMed: 24823376]
31. Asada N, Kunisaki Y, Pierce H, Wang Z, Fernandez NF, Birbrair A, Ma'ayan A, and Frenette PS (2017). Differential cytokine contributions of perivascular haematopoietic stem cell niches. Nat Cell Biol 19, 214–223. 10.1038/ncb3475. [PubMed: 28218906]
32. Kunisaki Y, Bruns I, Scheiermann C, Ahmed J, Pinho S, Zhang D, Mizoguchi T, Wei Q, Lucas D, Ito K, et al. (2013). Arteriolar niches maintain haematopoietic stem cell quiescence. Nature 502, 637–643. 10.1038/nature12612. [PubMed: 24107994]
33. Isern J, Garcia-Garcia A, Martin AM, Arranz L, Martin-Perez D, Torroja C, Sanchez-Cabo F, and Mendez-Ferrer S (2014). The neural crest is a source of mesenchymal stem cells with specialized hematopoietic stem cell niche function. Elife 3, e03696. 10.7554/eLife.03696. [PubMed: 25255216]
34. Tan Y, and Cahan P (2019). SingleCellNet: A Computational Tool to Classify Single Cell RNA-Seq Data Across Platforms and Across Species. Cell Syst 9, 207–213 e202. 10.1016/j.cels.2019.06.004. [PubMed: 31377170]
35. Shen B, Tasdogan A, Ubellacker JM, Zhang J, Nosyreva ED, Du L, Murphy MM, Hu S, Yi Y, Kara N, et al. (2021). A mechanosensitive peri-arteriolar niche for osteogenesis and lymphopoiesis. Nature 591, 438–444. 10.1038/s41586-021-03298-5. [PubMed: 33627868]
36. Bjorbaek C, Uotani S, da Silva B, and Flier JS (1997). Divergent signaling capacities of the long and short isoforms of the leptin receptor. J Biol Chem 272, 32686–32695. 10.1074/jbc.272.51.32686. [PubMed: 9405487]
37. Liu H, Du T, Li C, and Yang G (2021). STAT3 phosphorylation in central leptin resistance. Nutr Metab (Lond) 18, 39. 10.1186/s12986-021-00569-w. [PubMed: 33849593]
38. DeFalco J, Tomishima M, Liu H, Zhao C, Cai X, Marth JD, Enquist L, and Friedman JM (2001). Virus-assisted mapping of neural inputs to a feeding center in the hypothalamus. Science 291, 2608–2613. 10.1126/science.1056602. [PubMed: 11283374]
39. Stanley ER, and Chitu V (2014). CSF-1 receptor signaling in myeloid cells. Cold Spring Harb Perspect Biol 6. 10.1101/cshperspect.a021857.
40. Goodwin RG, Lupton S, Schmierer A, Hjerrild KJ, Jerzy R, Clevenger W, Gillis S, Cosman D, and Namen AE (1989). Human interleukin 7: molecular cloning and growth factor activity on human and murine B-lineage cells. Proc Natl Acad Sci U S A 86, 302–306. 10.1073/pnas.86.1.302. [PubMed: 2643102]
41. Meacham CE, Jeffery EC, Burgess RJ, Sivakumar CD, Arora MA, Stanley AM, Colby EM, Crane GM, Zhao Z, and Morrison SJ (2022). Adiponectin receptors sustain haematopoietic stem cells throughout adulthood by protecting them from inflammation. Nat Cell Biol 24, 697–707. 10.1038/s41556-022-00909-9. [PubMed: 35513711]
42. Luster AD, Unkeless JC, and Ravetch JV (1985). Gamma-interferon transcriptionally regulates an early-response gene containing homology to platelet proteins. Nature 315, 672–676. 10.1038/315672a0. [PubMed: 3925348]
43. Luster AD, Jhanwar SC, Chaganti RS, Kersey JH, and Ravetch JV (1987). Interferon-inducible gene maps to a chromosomal band associated with a (4;11) translocation in acute leukemia cells. Proc Natl Acad Sci U S A 84, 2868–2871. 10.1073/pnas.84.9.2868. [PubMed: 2437586]
44. Pandey V, Fleming-Martinez A, Bastea L, Doeppler HR, Eisenhauer J, Le T, Edenfield B, and Storz P (2021). CXCL10/CXCR3 signaling contributes to an inflammatory microenvironment and its blockade enhances progression of murine pancreatic precancerous lesions. Elife 10. 10.7554/eLife.60646.

45. Sun MY, Yetman MJ, Lee TC, Chen Y, and Jankowsky JL (2014). Specificity and efficiency of reporter expression in adult neural progenitors vary substantially among nestin-CreER(T2) lines. J Comp Neurol 522, 1191–1208. 10.1002/cne.23497. [PubMed: 24519019]
46. Zimmerman L, Parr B, Lendahl U, Cunningham M, McKay R, Gavin B, Mann J, Vassileva G, and McMahon A (1994). Independent regulatory elements in the nestin gene direct transgene expression to neural stem cells or muscle precursors. Neuron 12, 11–24. 10.1016/0896-6273(94)90148-1. [PubMed: 8292356]
47. Arranz L, Sanchez-Aguilera A, Martin-Perez D, Isern J, Langa X, Tzankov A, Lundberg P, Muntion S, Tzeng YS, Lai DM, et al. (2014). Neuropathy of haematopoietic stem cell niche is essential for myeloproliferative neoplasms. Nature 512, 78–81. 10.1038/nature13383. [PubMed: 25043017]
48. Mendez-Ferrer S, Michurina TV, Ferraro F, Mazloom AR, Macarthur BD, Lira SA, Scadden DT, Ma'ayan A, Enikolopov GN, and Frenette PS (2010). Mesenchymal and haematopoietic stem cells form a unique bone marrow niche. Nature 466, 829–834. 10.1038/nature09262. [PubMed: 20703299]
49. Fukushi J, Inatani M, Yamaguchi Y, and Stallcup WB (2003). Expression of NG2 proteoglycan during endochondral and intramembranous ossification. Dev Dyn 228, 143–148. 10.1002/dvdy.10359. [PubMed: 12950088]
50. Logan M, Martin JF, Nagy A, Lobe C, Olson EN, and Tabin CJ (2002). Expression of Cre Recombinase in the developing mouse limb bud driven by a Prxl enhancer. Genesis 33, 77–80. 10.1002/gene.10092. [PubMed: 12112875]
51. Comazzetto S, Murphy MM, Berto S, Jeffery E, Zhao Z, and Morrison SJ (2019). Restricted Hematopoietic Progenitors and Erythropoiesis Require SCF from Leptin Receptor+ Niche Cells in the Bone Marrow. Cell Stem Cell 24, 477–486 e476. 10.1016/j.stem.2018.11.022. [PubMed: 30661958]
52. Flanagan JG, Chan DC, and Leder P (1991). Transmembrane form of the kit ligand growth factor is determined by alternative splicing and is missing in the Sld mutant. Cell 64, 1025–1035. 10.1016/0092-8674(91)90326-t. [PubMed: 1705866]
53. Wolf NS (1978). Dissecting the hematopoietic microenvironment. III. Evidence for a positive short range stimulus for cellular proliferation. Cell Tissue Kinet 11, 335–345. [PubMed: 356997]
54. Buono M, Facchini R, Matsuoka S, Thongjuea S, Waithe D, Luis TC, Giustacchini A, Besmer P, Mead AJ, Jacobsen SE, and Nerlov C (2016). A dynamic niche provides Kit ligand in a stage-specific manner to the earliest thymocyte progenitors. Nat Cell Biol 18, 157–167. 10.1038/ncb3299. [PubMed: 26780297]
55. Liu Y, Chen Q, Jeong HW, Koh BI, Watson EC, Xu C, Stehling M, Zhou B, and Adams RH (2022). A specialized bone marrow microenvironment for fetal haematopoiesis. Nat Commun 13, 1327. 10.1038/s41467-022-28775-x. [PubMed: 35288551]
56. Oguro H, Ding L, and Morrison SJ (2013). SLAM family markers resolve functionally distinct subpopulations of hematopoietic stem cells and multipotent progenitors. Cell Stem Cell 13, 102–116. 10.1016/j.stem.2013.05.014. [PubMed: 23827712]
57. Zhang J, Wu Q, Johnson CB, Pham G, Kinder JM, Olsson A, Slaughter A, May M, Weinhaus B, D'Alessandro A, et al. (2021). In situ mapping identifies distinct vascular niches for myelopoiesis. Nature 590, 457–462. 10.1038/s41586-021-03201-2. [PubMed: 33568812]
58. Kisanuki YY, Hammer RE, Miyazaki J, Williams SC, Richardson JA, and Yanagisawa M (2001). Tie2-Cre transgenic mice: a new model for endothelial cell-lineage analysis in vivo. Dev Biol 230, 230–242. 10.1006/dbio.2000.0106. [PubMed: 11161575]
59. Zhu X, Bergles DE, and Nishiyama A (2008). NG2 cells generate both oligodendrocytes and gray matter astrocytes. Development 135, 145–157. 10.1242/dev.004895. [PubMed: 18045844]
60. Daigle TL, Madisen L, Hage TA, Valley MT, Knoblich U, Larsen RS, Takeno MM, Huang L, Gu H, Larsen R, et al. (2018). A Suite of Transgenic Driver and Reporter Mouse Lines with Enhanced Brain-Cell-Type Targeting and Functionality. Cell 174, 465–480 e422. 10.1016/j.cell.2018.06.035. [PubMed: 30007418]

61. Balordi F, and Fishell G (2007). Hedgehog signaling in the subventricular zone is required for both the maintenance of stem cells and the migration of newborn neurons. J Neurosci 27, 5936–5947. 10.1523/JNEUROSCI.1040-07.2007. [PubMed: 17537964]

62. Stuart T, Butler A, Hoffman P, Hafemeister C, Papalexi E, Mauck WM 3rd, Hao Y, Stoeckius M, Smibert P, and Satija R (2019). Comprehensive Integration of Single-Cell Data. Cell 177, 1888–1902 e1821. 10.1016/j.cell.2019.05.031. [PubMed: 31178118]

63. Cao J, Spielmann M, Qiu X, Huang X, Ibrahim DM, Hill AJ, Zhang F, Mundlos S, Christiansen L, Steemers FJ, et al. (2019). The single-cell transcriptional landscape of mammalian organogenesis. Nature 566, 496–502. 10.1038/s41586-019-0969-x. [PubMed: 30787437]

64. Yu G, Wang LG, Han Y, and He QY (2012). clusterProfiler: an R package for comparing biological themes among gene clusters. OMICS 16, 284–287. 10.1089/omi.2011.0118. [PubMed: 22455463]

Highlights

- HSCs were adjacent to sinusoidal blood vessels in early postnatal bone marrow (BM)
- LepR+ and endothelial cells had the highest *Scf* levels in postnatal BM
- SCF from LepR+ cells was required by myeloerythroid progenitors in postnatal BM
- SCF from endothelial cells was required for HSC maintenance in early postnatal BM

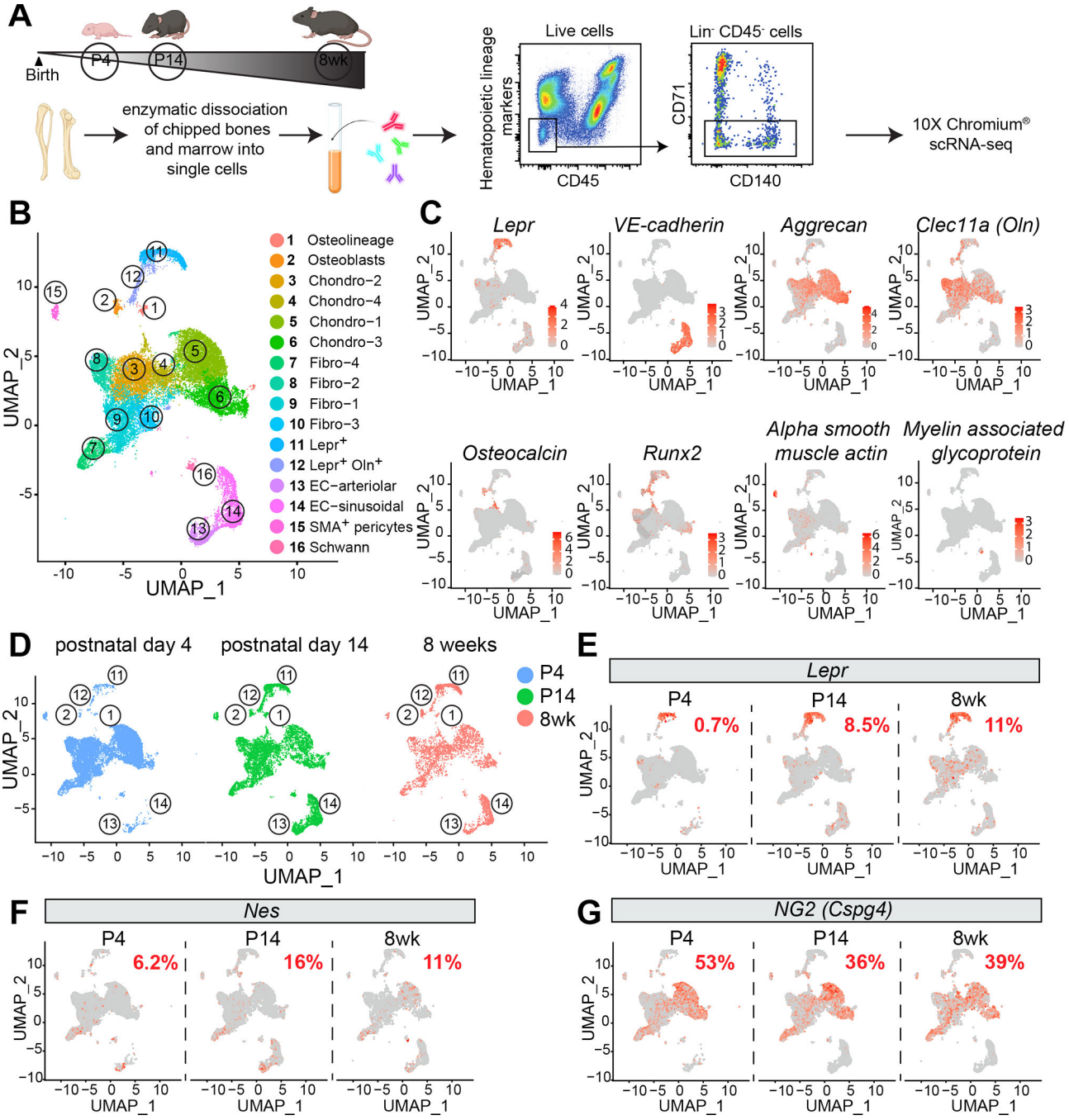

Figure 1. Single cell RNA sequencing of non-hematopoietic cells from early postnatal and adult mouse bone and bone marrow.

(A) Experimental design and flow cytometry gates used to isolate endothelial cells (CD140 negative) and stromal cells (CD140$^+$) that were negative for CD45, CD71, and hematopoietic lineage markers from enzymatically dissociated P4, P14, or 8 week-old femurs and tibias. The mouse images were derived from BioRender. (B) Uniform manifold approximation and projection (UMAP) plot showing cell clusters from analysis of 23,657 non-hematopoietic cells from enzymatically dissociated P4, P14, and 8 week-old bones/bone marrow. (C) UMAP plots for the expression of genes that mark bone marrow stromal

cell types listed in panel B. (D) UMAP plots of cells from P4, P14 and 8 week-old bones/bone marrow. (E-G) UMAP plots showing the expression of *Lepr* (E), *Nestin* (F), and *NG2 (Cspg4)* (G) in stromal cells from P4, P14 and 8 week-old bones/bone marrow. The percentages in panels E to G represent the mean percentages of cells that were positive for the indicated transcripts. See also Figure S1, S2, S3 and Table S1.

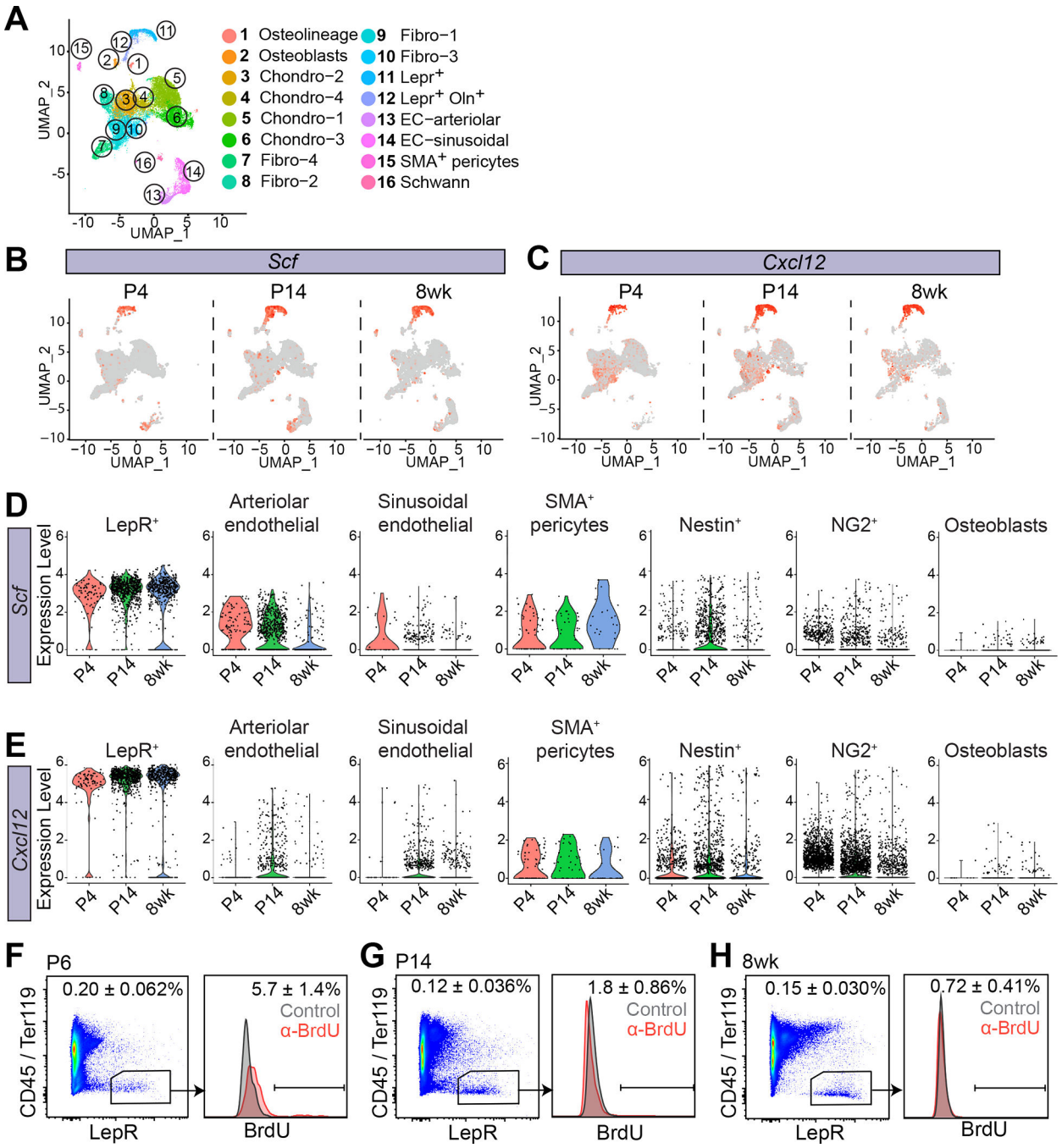

Figure 2. Expression patterns of *Scf* and *Cxcl12* niche factors by single cell RNA sequencing in non-hematopoietic cells from early postnatal and adult bone/bone marrow.

(A) UMAP visualization of all non-hematopoietic cell clusters from P4, P14 and 8 week-old bones/bone marrow. (B, C) UMAP plots showing *Scf* (B) and *Cxcl12* (C) expression. (D, E) Violin plots showing the expression patterns of *Scf* (D) and *Cxcl12* (E) in *Lepr*$^+$ stromal cells, arteriolar and sinusoidal endothelial cells, *SMA*$^+$ pericytes, *Nestin*$^+$ stromal cells, *NG2*$^+$ stromal cells and osteoblasts from P4, P14 and 8 week-old bones/bone marrow. (F-H) Incorporation of a 2 hour pulse of BrdU by LepR$^+$ cells from enzymatically dissociated bone/bone marrow from P6 (F), P14 (G) and 8-week-old mice (H) (a total of 5–6 mice per

time point from 2 independent experiments per time point). All data reflect mean±standard deviation. See also Figure S3.

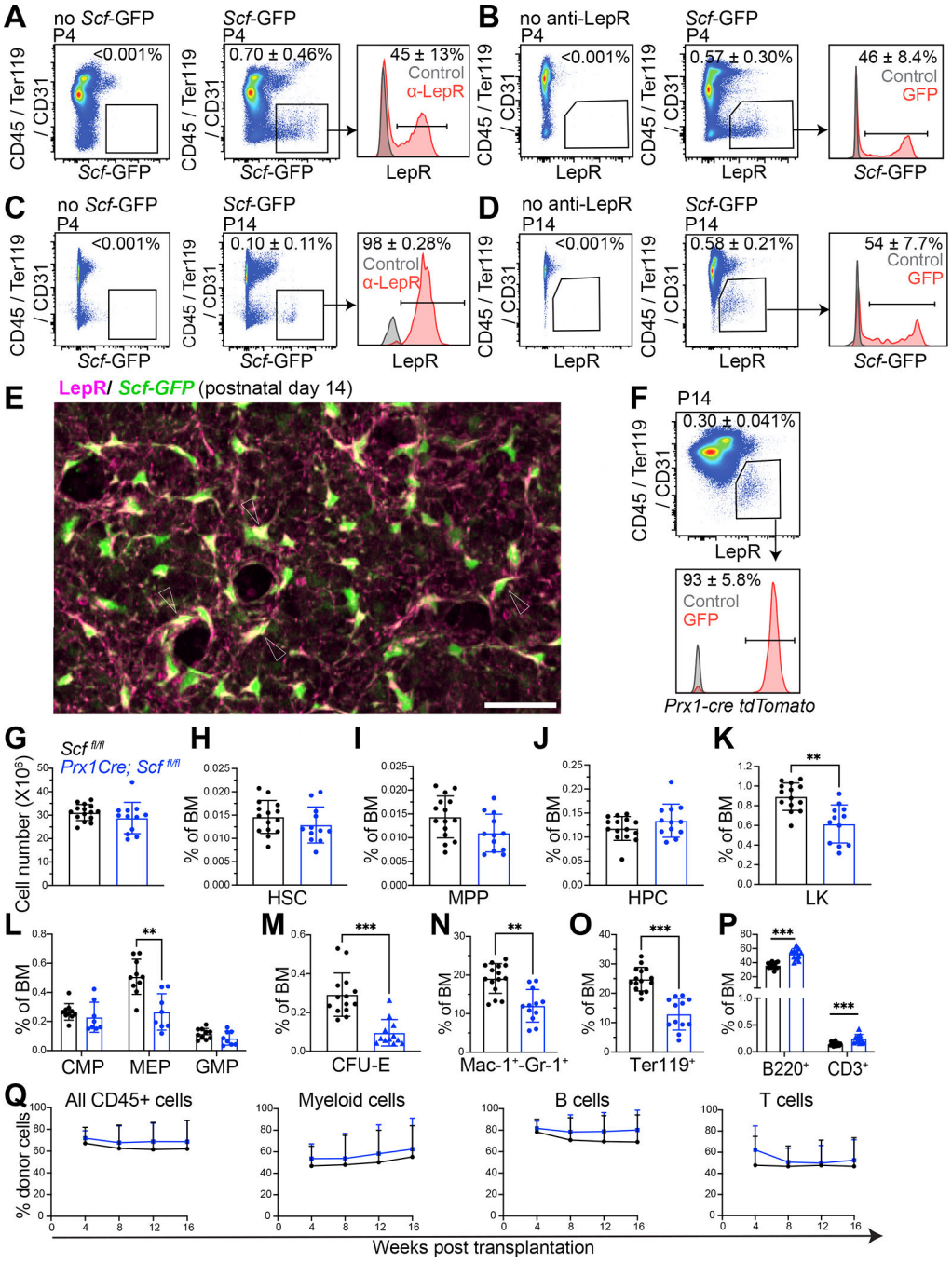

Figure 3. SCF from LepR$^+$ cells promotes myelopoiesis and erythropoiesis in early postnatal marrow.

(A-D) Analysis of enzymatically dissociated tibia and femur from *Scf*-GFP mice at P4 (A, B) and P14 (C, D) (a total of 5 mice per time point from 2 independent experiments per time point). The first panels in A and C are from negative control bone marrow lacking *Scf*-GFP. The other panels show the percentage of *Scf*-GFP$^+$ stromal cells (negative for CD45, Ter119 and CD31) that were LepR$^+$ at P4 (A) and P14 (C). Panels B and D show the percentage of LepR$^+$ cells that were *Scf*-GFP$^+$ at P4 (B) and P14 (D) (the first panel is a negative control lacking anti-LepR antibody staining). (E) Image of P14 femur bone

marrow showing that most LepR$^+$ cells were *Scf*-GFP$^+$ (arrowheads point to LepR$^+$*Scf*-GFP$^+$ cells; representative of two independent experiments). (F) Flow cytometric analysis of Tomato expression by LepR$^+$ bone marrow cells from *Prx1-cre; tdTomato* mice at P14 (representative of 3 mice from 2 independent experiments). (G-P) Bone marrow (two femurs and two tibias) cellularity (G) as well as the frequencies of HSCs (H), MPPs (I), HPCs (J), LK myeloid progenitors (K), CMPs, MEPs, GMPs (L), CFU-Es (M), Mac-1$^+$Gr-1$^+$ myeloid cells (N), Ter119$^+$ erythroid cells (O), B220$^+$ B cells and CD3$^+$ T cells (P) in the bone marrow of *Prx1-cre; Scf* $^{fl/fl}$ and littermate control mice at P14 (n=8–15 mice per genotype from 6 independent experiments; each dot represents a different mouse). (Q) Donor-derived reconstitution in the blood of mice competitively transplanted with *Prx1-cre; Scf* $^{fl/fl}$ or control donor bone marrow cells (2 donors per genotype were transplanted into a total of 10 recipients per genotype in two independent experiments). All data represent mean ± standard deviation. *p<0.05; **p<0.01; ***p<0.001 from Welch's t-test (G), Student's t-tests followed by Holm-Sidak multiple comparisons adjustments (H-P), Student's t-tests or Mann-Whitney tests followed by Holm-Sidak multiple comparisons adjustments and non-parametric analysis of longitudinal data, nparLD (Q). All statistical tests were two-sided. See also Figure S4, S5, S6, Table S2 and Table S3.

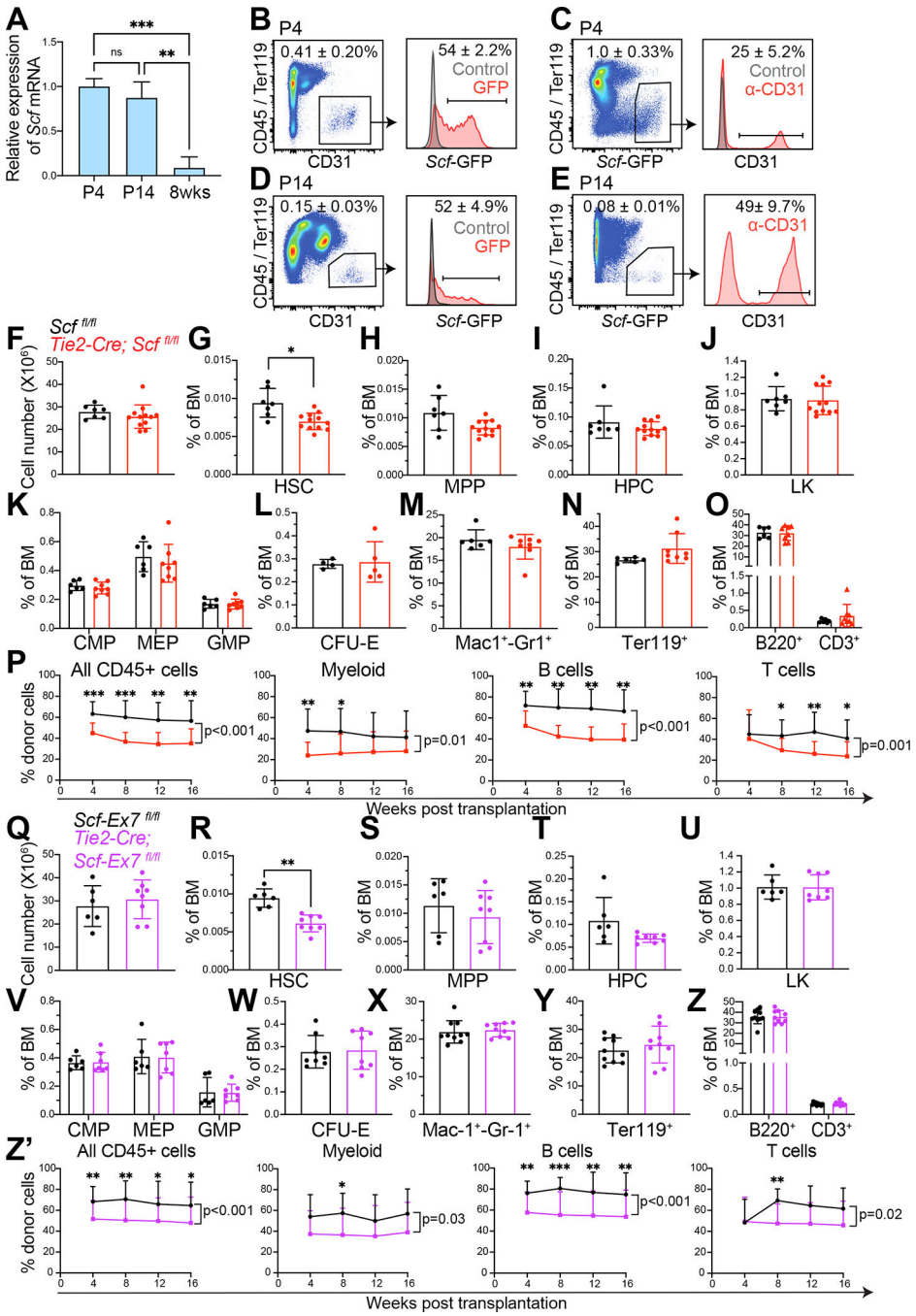

Figure 4. SCF from endothelial cells promotes HSC maintenance in early postnatal bone marrow.

(A) Quantitative RT-PCR (qRT-PCR) analysis of *Scf* levels in CD45^{-}Ter119^{-}CD31^{+} endothelial cells from P4, P14 and 8 week-old bone marrow. Data were normalized to *Scf* levels at P4 (n=6–9 mice per time point from 3 independent experiments per time point). (B-E) Flow cytometric analysis of *Scf*-GFP expression by endothelial cells from enzymatically dissociated femurs and tibias from P4 (B, C) and P14 (D, E) mice (n=5–6 mice per time point from 2–3 independent experiments per time point). (F-O) Bone marrow (two femurs and two tibias) cellularity (F) as well as the frequencies of HSCs (G),

MPPs (H), HPCs (I), LK myeloid progenitors (J), CMPs, MEPs, GMPs (K), CFU-Es (L), Mac-1^+Gr-1^+ myeloid cells (M), Ter119^+ erythroid cells (N), B220^+ B cells and CD3^+ T cells (O) in the bone marrow of *Tie2-cre; Scf* $^{fl/fl}$ and littermate control mice at P14 (n=4–12 mice per genotype from 3–4 independent experiments). (P) Donor-derived cells in the blood of mice competitively transplanted with *Tie2-cre; Scf* $^{fl/fl}$ or control donor bone marrow cells (3 donors per genotype were transplanted into a total of 15 recipients per genotype in three independent experiments). (Q-Z) Bone marrow (two femurs and two tibias) cellularity (Q) as well as the frequencies of HSCs and restricted hematopoietic progenitors (R-Z) in the bone marrow of *Tie2-cre; Scf-Ex7* $^{fl/fl}$ and littermate control mice at P14 (n=6–10 mice per genotype from 3 independent experiments). (Z') Donor-derived cells in the blood of mice competitively transplanted with *Tie2-cre; Ex7-Scf* $^{fl/fl}$ or control donor bone marrow cells (4 donors per genotype were transplanted into a total of 18 recipients per genotype in four independent experiments). All data represent mean ± standard deviation. The statistical significance of differences among groups (*p<0.05; **p<0.01; ***p<0.001) was assessed using a one-way ANOVA followed by Tukey's multiple comparisons adjustments (A), Student's t-tests (F, Q), Mann-Whitney tests followed by Holm-Sidak's multiple comparisons adjustments (G-O; R-Z), Student's t-tests or Mann-Whitney tests followed by Holm-Sidak multiple comparisons adjustments (P, Z'), or non-parametric analysis of longitudinal data, nparLD (P, Z'). All statistical tests were two-sided. See also Figure S6, Table S2 and Table S3.

Key resources table

REAGENT or RESOURCE	SOURCE	IDENTIFIER
Antibodies		
Purified Rat α-Mouse CD16/CD32 (Mouse BD Fc Block™)	BD Biosciences	Cat. 553142
α-mouse CD34 Biotin	eBioscience	clone RAM34; RRID:AB_466425
α-mouse CD71 PE	Biolegend	clone R17217; RRID:AB_465741
α-mouse CD71 BV421	Biolegend	clone R17217; RRID:AB_10899739
α-mouse CD45 APC	Tonbo Biosciences	clone 30-F11;
α-mouse CD45 PE-Cy7	Tonbo Biosciences	clone 30-F11;
α-mouse CD2 APC	Tonbo Biosciences	clone RM2-5; RRID: AB_2563090
α-mouse CD2 PE	Tonbo Biosciences	clone RM2-5; RRID:AB_2621728
α-mouse CD3 APC	Tonbo Biosciences	clone 17A2; RRID:AB_2621538
α-mouse CD3 PE	Tonbo Biosciences	clone 17A2; RRID:AB_2621731
α-mouse CD3 redFluor™700	Tonbo Biosciences	clone 17A2; RRID: AB_2621971
α-mouse CD5 APC	Biolegend	clone 53-7.3;RRID:AB_2563929
α-mouse CD5 PE	Biolegend	clone 53-7.3; RRID:AB_312736
α-mouse CD8a APC	Biolegend	clone 53-6.7; RRID:AB_312751
α-mouse CD8a PE	Tonbo Biosciences	clone 53-6.7; RRID:AB_2621741
α-mouse CD11b APC	eBioscience	clone M1/70; RRID:AB_469344
α-human/mouse CD11b PE	Biolegend	clone M1/70; RRID:AB_312790
α-mouse CD11b APC-eFluor780	eBioscience	clone M1/70; RRID:AB_1603193
α-mouse Gr1 APC	Tonbo Biosciences	clone RB6-8C5; RRID:AB_2621610
α-mouse Gr1 PE	Tonbo Biosciences	clone RB6-8C5; RRID:AB_2621803
α-mouse Gr1 PE-Cy7	Biolegend	clone RB6-8C5; RRID:AB_313381
α-mouse Gr1 Alexa Fluor700	Biolegend	clone RB6-8C5;RRID: AB_2137487
α-mouse Gr1 BV510	Biolegend	clone RB6-8C5; RRID:AB_2650931
α-human/mouse B220 APC	Tonbo Biosciences	clone RA3-6B2; RRID:AB_ 2621574
α- human/mouse B220 PE	Tonbo Biosciences	clone RA3-6B2; RRID:AB_2621764
α- human/mouse B220 Percp-Cy5.5	Tonbo Biosciences	clone RA3-6B2; RRID:AB_2621892
α-mouse Ter119 APC	Tonbo Biosciences	clone TER-119; RRID:AB_2621609
α-mouse Ter119 PE	Tonbo Biosciences	clone TER-119; RRID:AB_2621802
α-mouse Ter119 PE-Cy7	Biolegend	clone TER-119; RRID:AB_2281408
Streptavidin BV421	Biolegend	Cat. No. 405226
Streptavidin BV510	Biolegend	Cat. No. 405234
α-mouse CD45.1 PE-Cy7	Tonbo Biosciences	clone A20; RRID:AB_2621850
α-mouse CD45.2 VioletFluor 450	Tonbo Biosciences	clone 104; RRID:AB_2621950
α-mouse CD150 BV421	Biolegend	Clone TC15-12F12.2; RRID:AB_10896787
α-mouse CD48 Alexa Fluor700	Biolegend	clone HM48-1; RRID:AB_10612754
α-mouse cKit APC-eFluor780	eBioscience	clone 2B8; RRID:AB_1272177

REAGENT or RESOURCE	SOURCE	IDENTIFIER
α-mouse IL7Rα(CD127) PE-Cy7	Tonbo Biosciences	clone A7R34; RRID:AB_2621859
α-mouse Flt3(CD135) APC	Biolegend	clone A2F10; RRID:AB_2107050
α-mouse Sca1 Percp-Cy5.5	eBioscience	Clone D7; RRID:AB_1272177
α-mouse CD43 PE	BD Biosciences	clone S7; RRID:AB_394748
α-mouse IgM APC	eBioscience	clone Il/41; RRID:AB_469458
α-mouse CD105 APC	Biolegend	clone MJ/78; RRID:AB_2687060
α-mouse CD41 PE-Cy7	Biolegend	clone MWReg30; RRID:AB_11124102
α-mouse CD16/32 (FcgRIII/II) Alexa Fluor700	eBioscience	clone 93; RRID:AB_493994
α-mouse CD31 PE	Biolegend	clone 390; RRID:AB_312903
α-mouse CD31 APC	Biolegend	clone 390; RRID:AB_312905
α-mouse VE-cadherin (CD144) efluor660	eBioscience	clone BV13; RRID:AB_11219483
Ghost Dye™ Red 780	Tonbo Biosciences	Cat. 13-0865
Goat α-mouse LepR antibody, Biotin	R&D System	BAF497; RRID:AB_2296953
Goat α-mouse CD117/c-kit antibody	R&D System	BAF1356; RRID:AB_ 355961
Goat α-CD105 antibody	R&D System	Cat. AF1320
Rabbit α-NG2 antibody	Sigma Aldrich	Cat. AB5320
Rabbit α-Aggrecan antibody	Sigma Aldrich	Cat. AB1031
Rabbit α-dsRed/tdTomato antibody	Takara	Cat. 632496
Rabbit α-Laminin 1+2 antibody	Abcam	Cat. ab7463
Rabbit α-CD105 antibody	Abcam	Cat. ab221675
Chicken α-Green Fluorescent Protein antibody	Aves Labs	Cat. GFP-1020
Donkey α-rabbit IgG (H+L) Alexa Fluor 488	Jackson ImmunoResearch	Cat. 711-545-152
Donkey α-chicken IgG (H+L) Alexa Fluor 647	Jackson ImmunoResearch	Cat. 703-606-155
Donkey α-goat IgG (H+L) Alexa Fluor 555	Thermo Fisher Scientific	Cat. A21432; RRID:AB_2535853
Chemicals, peptides, and recombinant proteins		
HI bovine serum (FBS)	Thermo Fisher Scientific	Cat. 26170043
Hank's Balanced Salt Solution (HBSS)	Thermo Fisher Scientific	Cat. MT21022CV
DNase I	Sigma-Aldrich	Cat. 10104159001
Liberase™ TL	Sigma-Aldrich	Cat. 05401020001
Benzyl alcohol	Sigma-Aldrich	Cat. 305197
Benzyl benzoate	Thermo Fisher Scientific	Cat. AC105860010
Corn oil	Sigma-Aldrich	Cat. C8267
Tamoxifen	Sigma-Aldrich	Cat. T5648
NP-40	Sigma- Aldrich	Cat. I8896
Donkey serum	Jackson ImmunoResearch	Cat. 017-000-121
DMSO	Sigma-Aldrich	Cat. D4540
4% Paraformaldehyde in PBS	Thermo Fisher Scientific	Cat. AAJ19943K2
iScript™ Reverse Transcription Supermix for RT-qPCR	Bio-Rad	Cat.1708840
iTaq Universal SYBR Green Supermix	Bio-Rad	Cat. 172-5124

REAGENT or RESOURCE	SOURCE	IDENTIFIER
Critical commercial assays		
Chromium Next GEM Single Cell 3' GEM, Library & Gel Bead Kit v3.1	10X Genomics	Cat. PN-1000128
Chromium Next GEM Chip G Single Cell Kit	10X Genomics	Cat. PN-1000127
Chromium i7 Multiplex Kit	10X Genomics	Cat. PN PN-120262
Invitrogen Qubit Assay Tubes	Thermo Fisher Scientific	Cat. Q32856
Qubit dsDNA HS Assay Kit	Thermo Fisher Scientific	Cat. Q32851
High Sensitivity D1000 Screen Tape	Agilent Technologies	Cat. 5067-5584
High Sensitivity D1000 Reagents	Agilent Technologies	Cat. 5067-5585
Deposited data		
single cell RNA sequencing data	This paper	BioProject ID: PRJNA835050 https://dataview.ncbi.nlm.nih.gov/object/PRJNA835050?reviewer=4834apu817huim2i1uoq9afl14
Code	This paper	https://git.biohpc.swmed.edu/CRI/morrison-lab/scRNASeq/
Experimental models: Organisms/strains		
Scf^{GFP} (Kitl$^{tm1.1Sjm}$/J)	Ding et al.[12]	RRID:IMSR_JAX:017860
Scf^{FL} (Kitl$^{tm2.1Sjm/J}$)	Ding et al.[12]	RRID:IMSR_JAX:017861
Kitl$^{LEx7/Lex7}$*(Scf-Ex7*$^{fl/fl}$*)*	Buono et al.[54]	N.A.
Tie2-cre (B6.Cg-Tg(Tek-cre)1Ywa/J)	Kisanuki et al.[58]	RRID: IMAR_JAX:008863
Prx1-cre (B6.Cg-Tg(Prrx1-cre)1Cjt/J)	Logan et al.[50]	RRID:IMSR_JAX:005584
Lepr-cre (B6.129(Cg)-Lepr$^{tm2(cre)Rck}$/J)	DeFalco et al.[38]	RRID:IMSR_JAX:008320
Nestin-cre (B6.Cg-Tg(Nes-cre)1Kln/J)	Jackson Laboratory	RRID:IMSR_JAX:003771
NG2-creER (B6.Cg-Tg(Cspg4-cre/Esr1)BAkik/J)	Jackson Laboratory	RRID:IMSR_JAX: 008538
Rosa26-tdTomato (B6.Cg-Gt(ROSA)26Sor$^{tm9(CAG-tdTomato)Hze}$/J) (tdTomato)	Jackson Laboratory	RRID:IMSR_JAX:007909
Nestin-creER	Balordi and Fishell,[61]	N.A.
NG2-cre (B6; FVB-Ifi208-Tg(Cspg4-cre)1Akik/J)	Zhu et al.[59]	RRID:IMSR_JAX:008533
α-catulin^{GFP} (*Ctnna1*$^{tm1.1Sjm}$/J)	Acar et al.[8]	RRID:IMSR_JAX:028342
Gt(ROSA)26Sor$^{tm47(CAG-EGFP*)Hze}$/J (Ai47-GFP)	Daigle et al.[60]	N.A.
Oligonucleotides		
See Table S4 for list of qRT-PCR and genotyping primers used in this study	Integrated DNA Technologies	N.A.
Software and algorithms		
Cell Ranger single cell software suite v.4.0	10X Genomics	RRID: SCR_017344
FlowJo v.10.4	Flowjo, LLC	RRID: SCR_016768
BD FACSDiva	BD Biosciences	RRID: SCR_001456
Graphpad Prism v.9.1.0	Graphpad	RRID: SCR_002798
Imaris Bitplane v.8.2	Bitplane	RRID: SCR_007370
Imaris Bitplane v.9.9	Bitplane	RRID: SCR_007370

REAGENT or RESOURCE	SOURCE	IDENTIFIER
R 4.0.2	R Project	RRID: SCR_001905
Seurat 3.2	Stuart et al.[62]	RRID: SCR_016341
clusterProfiler 3.18.1	Yu et al.[64]	RRID: SCR_016884
Monocle 3	Cao et al. [63]	RRID: SCR_018685